Ocean and Coastal Management 253 (2024) 107157

Contents lists available at ScienceDirect

Ocean and Coastal Management

journal homepage: www.elsevier.com/locate/ocecoaman

Pebble tracing experiment at the Promenade des Anglais (Nice, France): A contribution towards beach management efforts

Duccio Bertoni [a,*], Silas Dean [a], Alessandro Pozzebon [b], Rémi Dumasdelage [c], Julien Larraun [c], Giovanni Sarti [a]

[a] Dipartimento di Scienze della Terra, University of Pisa, via Santa Maria 53, 56126, Pisa, Italy
[b] Dipartimento di Ingegneria dell'Informazione, University of Padua, via Gradenigo 6/b, 35131, Padua, Italy
[c] Service Etudes et Travaux Ports et Littoral, Metropole Nice Côte d'Azur, 1 route de grenoble, Nice, France

ARTICLE INFO

Keywords:
Coarse sediments
Pebble shape
Coastal management
Nourishment
Wave simulation model
RFID technology

ABSTRACT

In this paper, the results of a short-term tracing experiment carried out at a beach compartment along the Bay of Nice (southern France) are presented. Nice urban beach is characterized by persistent offshore sediment loss issues that force the local administration to operate frequent artificial replenishments to maintain the current configuration, which also protects the well-renown Promenade des Anglais from high-energy events. As beach refills are quite expensive, the aim of the paper is to provide novel insights about the transport processes of pebble-sized tracers, which might support the Municipality to better adjust future interventions. Pebbles were tracked by means of the Radio Frequency Identification technology, largely used in such settings because of its reliability and efficiency. In addition, the morphology of the beach was monitored during the three-days-long experiment by airborne and ground topographic surveys, as well as the shape and the size of the tracers. Finally, a wave model was produced to simulate wave propagation in the nearshore, which validates the observed transport patterns. The results documented a low recovery rate (56%) 4 h after tracer injection, which is uncharacteristic considering that it jumped to 91% after the second survey, 24 h after the injection. At the end of the experiment (48 h), the recovery rate sank to 14%. These data were adequate to identify a few trends in pebble transport: tracer recovery rate in the swash zone was very low, while many marked pebbles were found at the step crest. Although this transport pattern may corroborate the offshore movement of the sediments, the topographic surveys revealed the destruction and re-formation of the fair-weather berm overnight, which would imply the presence of a shoreward transport under low energy wave conditions. While size did not single out any tendency, shape did: spheres rolled down the beachface earlier than disks; by contrast, disk-shaped pebbles moved for longer distances than spheres. These findings will be useful for local coastal managers because next beach fills will be planned and optimized based on the observed transport patterns. Though the selection of disk-shaped pebbles implies increasing costs, replenishments would be more efficient and fine-tuned for this sector of coast, which would ultimately save resources reducing negative impacts on the environment along the way. These considerations are valid for the Bay of Nice, but they might be useful wherever coarse-clastic beaches need recurring replenishments.

1. Introduction

The management of urban beaches has been a focus of scientific literature in recent years (e.g., Cervantes et al., 2008; García-Morales et al., 2018; Rodella et al., 2019; Jolivet et al., 2022) because of the twofold significance of this environmental setting: i) a wide, healthy beach provides direct and indirect profits from tourism, which is usually the main income for coastal communities, and especially in the Mediterranean, and ii) a wide, healthy beach also protects inland areas by acting as a buffer against storms and, in the longer term, against sea-level rise. A non-healthy beach can also be useful because it is often protected by many defensive constructions that prevent further coastal retreat, while keeping revenue from tourism alive if the area is maintained by beach nourishments (e.g., Luo et al., 2016; Pranzini et al.,

* Corresponding author.
E-mail addresses: duccio.bertoni@unipi.it (D. Bertoni), silas.dean@dst.unipi.it (S. Dean), alessandro.pozzebon@unipd.it (A. Pozzebon), remi.dumasdelage@ville-nice.fr (R. Dumasdelage), julien.larraun@ville-nice.fr (J. Larraun), giovanni.sarti@unipi.it (G. Sarti).

https://doi.org/10.1016/j.ocecoaman.2024.107157
Received 13 September 2023; Received in revised form 8 April 2024; Accepted 8 April 2024
Available online 13 April 2024

2018; Cappucci et al., 2020; Pinto et al., 2020). It is widely accepted that the rigid structures as coastal protection must be used only as a last resort, because they have numerous downsides in adjacent sectors of the coast (French, 2001). Where environmental conditions do not allow a change to an approach that relies mainly on beach nourishments, nature-based, eco-engineering solutions can be adopted to mitigate erosion effects and enhance coastal protection (Morris et al., 2018). However, the combined implementation of nature-based structures (e.g., restored dunes, living seawalls, native intertidal vegetation) and nourishments is often perceived as key to optimal coastal zone management in areas where beach fills are not enough to counter coastline retreat (Schoonees et al., 2019). Nourishing activities may not represent the ultimate solution either: beside their cost and the need for frequent repetitions, they also pose questions about the source of the new sediments, their availability, their compatibility with native particles, environmental issues, and even potential long-term impacts along the coast (de Schipper et al., 2021). Regardless of their efficacy as a potential strategy to reduce the effects of climate change induced sea-level change (Parkinson and Ogurcak, 2018), especially considering "Endgame" future scenarios (Kemp et al., 2022), beach fills are the coastal protection practice most frequently used worldwide (e.g., Hanson et al., 2002; Cooke et al., 2012; Elko et al., 2021).

Among these coastal protection practices, nourishments made with coarse sediments are not uncommon because gravel and pebbles provide more stability than sand (Buscombe and Masselink, 2006). They are regularly used to refill eroding native coarse-clastic beaches (e.g., López et al., 2018; Tadić et al., 2022), and they are also increasingly used where the shore was originally sandy (e.g., Kumada et al., 2010; Bertoni et al., 2012). Another case of recurrent beach filling comes from the French Riviera in the Mediterranean (southeastern France): The sea-front of Nice, which is one of the most populated cities in France, and includes the well-known Promenade des Anglais in Nice. This area is characterized by a lengthy coarse-clastic beach that has been subject to many nourishment activities in the last decades (Anthony, 1997; Anthony et al., 2011). The decrease in sediment input of nearby rivers and the chronic offshore loss of gravel from the beach led local authorities to opt for beach nourishments along with broader protection plans that involved restoring riverbeds and coastal structures such as seawalls and groynes (Anthony and Julian, 1999). According to Anthony et al. (2011), the largest portion of fill sediments was collected from nearby construction sites, exploiting the building boom of recent decades. They were also collected from other interventions along riverbeds that were already underway. Both of these sources provided appropriate sediment since they were located along the rivers that naturally fed the beach. The acquisition price was low consisting mostly of transit costs. Since 2010 local authorities have been obliged to purchase gravel and pebbles from a more distant quarry (about 100 km away), which increased the cost of the beach maintenance significantly (Dumasdelage et al., 2016). The authors also stated that the offshore transport cannot represent the sole factor responsible for the documented loss of sediments: some other process contribute to the nearshore dynamics at Nice beach (e.g., longshore sediment redistribution or sediment mass loss).

Though much research has been taking place in recent times (e.g., Han et al., 2017; Pikelj et al., 2018; Eyal et al., 2021; Soloy et al., 2022), coarse-clastic beach processes are still under-investigated. The aim of the paper is to provide novel, additional data for local coastal managers by carrying out the first-ever pebble tracing experiment at the Promenade des Anglais. Such experiments have been successfully performed in many sites and settings worldwide (e.g., Allan et al., 2006; Dickson et al., 2011; Bertoni et al., 2012; Stark and Hay, 2016). The information about transport patterns would support the management of the beach and help optimize resources in terms of filling sediments. Considering the long experience of nourishments at the Nice beach, these insights may also be helpful to other municipalities implementing artificial gravel beaches as part of their coastal management strategies.

2. Study area

The city of Nice is located in the south-eastern sector of the Mediterranean coast of France in the Alpes-Maritimes department (Fig. 1a). Nice's urban beach is in the Bay of Nice on the eastern side of the 30 km-long Baie des Anges, which is one of the embayments of the French Riviera and corresponds to the depressed area of the continental margin between Cap d'Antibes and Cap Ferrat (Pupin et al., 2001). The French Riviera is the maritime edge of the French side of the Alps. It is characterized by narrow gravel beaches and a steep shoreface, which is the transition between the Alps and the Mediterranean Sea (Anthony, 1997). The seafloor is characterized by many submarine canyons, whose proximal edge is close to the shoreline due to the steepness of the shoreface. These canyons are the protraction of local coastal streams flowing into the Mediterranean Sea during the Messinian (Anthony et al., 2011; Barale, 2016).

The Bay of Nice is bounded by two headlands, Cap of Nice to the northeast and by the Var River delta to the southwest (Fig. 1a): no sediment exchange with adjacent sectors is feasible at either edge (Anthony, 1997; Anthony et al., 2011). The gravel beach that rims the Bay of Nice has been described as a barrier system formed by the sediments supplied by the Var River consisting of limestone pebbles and gravel derived from Pliocene deltaic puddingstones that the river intersects especially in the lower part of its catchment (Dubar and Anthony, 1995). Other minor streams contributed to the sediment supply of this coastal area: among them the Paillon and the Magnan rivers must be mentioned as they flow into the Bay of Nice. They are modified by human interventions though, and their sediment input is virtually negligible compared to the 100,000 m^3 gravel load of the Var River reported by Anthony and Julian (1999). The prevalent grain-size is on average 5–10 cm in diameter. Dumasdelage et al. (2016) document that grain-size decreases seaward along the shoreface, finer sediments such as sand may be typical for depths between −5 and −10 m. The Bay of Nice has a steep slope (ca. 10% between 0 and -20 m) that gets steeper between −20 m and −100 m (up to 80%).

The sea conditions in Southeast France are characterized by a microtidal environment (tidal range lower than 0.5 m) and by low-energy wind waves with a rather short fetch. High-energy events are typical of fall and winter seasons (Anthony et al., 2011; Dumasdelage et al., 2016). The average offshore wave height is about 0.8 m. Wave height during storms can reach a maximum of 6 m with a 100-year return period, which decreases to 4 m over a 10-year return period. According to the record of the CANDHIS Nice buoy (1.7 km offshore the Nice airport), the most frequent wave directions recorded in the period June 2002–March 2014 are south (157.5°N to 202.5°N, 65% of the dataset) and east-south-east (90°N to 135°N, 35% of the dataset). The mean significant height recorded by the buoy is 0.4 m (third quartile = 0.75 m) (Dumasdelage et al., 2014). Such a different approach of incident waves, coupled to the steep shoreface which prevents wave refraction, creates a bidirectional longshore drift in the embayment based on the prevalent wave propagation (Anthony et al., 2011).

The growth of the gravel beach in the Bay of Nice is connected to the recent evolution of the Var River delta, which has mostly been driven by anthropogenic activities (Anthony and Julian, 1999). The construction of the Nice-Côte d'Azur airport reclaimed a significant amount of land on the left side of the delta and as a result the eastward sediment supply from the river to the beach stopped. The bedload discharge of all the streams was already decreased because of waterworks (e.g., weirs) built along the riverbeds, dredging activities for construction notwithstanding. The natural sediment input was close to zero (Anthony et al., 2011) until authorities decided to remove the weirs, after which river sediment transport started to increase in recent times, and accretion was observed at the Var River delta. Progressive urbanization of the surrounding area led to the development of one of the most famous sea-fronts in the world, the Promenade des Anglais (Fig. 2a). The huge seawall at the back of the beach limited the beach width and likely

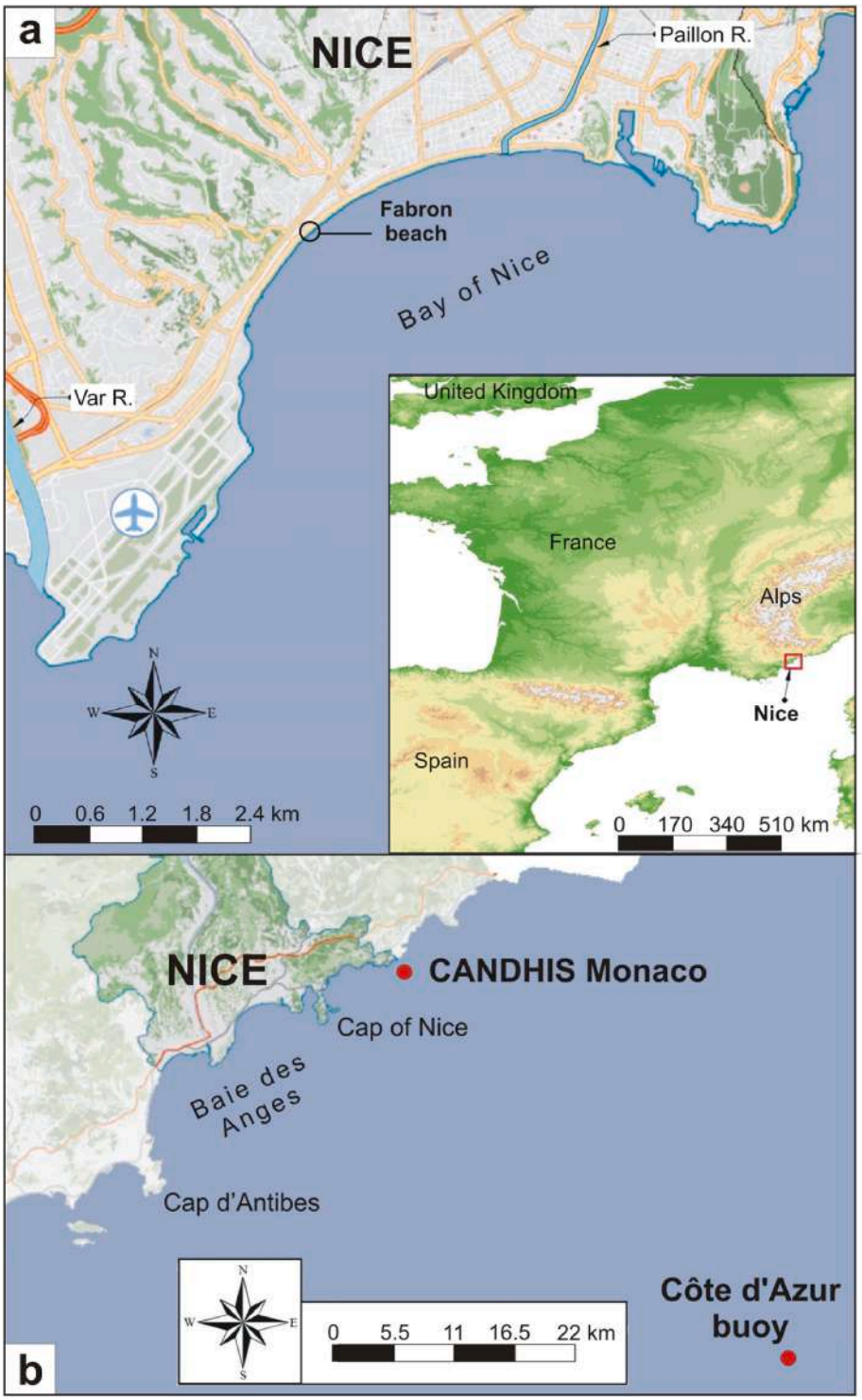

Fig. 1. Map of the study area with the exact location of the experiment site, the compartment named Fabron beach (a); close-up of the Baie des Anges: the red dots represent the location of the two referenced wave buoys (b).

induced strong seaward-directed transport processes of coarse sediments during storms. Due to the steepness of the seafloor fronting the shoreline, these sediments cannot be entrained and moved back to the beachface between the step and the crest of the berm. Such a loss, roughly quantified in 15,000 m^3/yr (SOGREAH, 2009), forced local coastal managers to intervene with frequent seasonal nourishments to balance the sediment budget. Between 1969 and 2015 about 600.000 m^3 of coarse sediments (prevalent grain-size 20–80 mm) have been used as beach fill (Dumasdelage et al., 2016). The investment is high, but the income generated by exploitation of the beach for tourism is clearly higher all year round, and Nice has increasingly become the center of economic development of the area. Along with soft defense activities such as nourishments, many hard groins made of large boulders have also been built to reduce the longshore transport of sediments, creating a series of short beach compartments along the embayment. The groins are more closely spaced in the southwestern sector of the beach, whereas they are more dispersed on the northeastern side. The tracing experiment was carried out in one of these compartments, located just more

Fig. 2. View of the Promenade des Anglais (a) and picture of the experiment site, the Fabron beach (b).

than 1 km from the southwestern edge of the Bay of Nice (Fig. 2b). This compartment, named Plage Fabron (hereafter referred to as Fabron beach), was selected because it is approximately 100 m long and confined between two large groins, which are expected to prevent or reduce longshore coarse sediment leakage, especially under the wave conditions in which the experiment was performed. A longer compartment would have provided more scattered results in terms of tracer recovery rate, thus decreasing the reliability of the dataset.

3. Methodology

The sampling phase took place in November 2019, when 130 limestone pebbles were collected on Fabron beach. The tracing experiment was carried out from January 13th, 2020 to January 15th, 2020. These dates were chosen based on the weather forecast: low wave energy was predicted, as the goal was to study coarse sediment movement during a fair-weather period in accordance with the existing literature: gravel and pebbles move extensively during high-energy events (e.g., Almeida et al., 2015; Grottoli et al., 2019; Ions et al., 2021), and they also move while wave motion is low as well (Bertoni et al., 2013; Grottoli et al., 2015). In addition, January corresponds to a period of relatively low beach use compared to the rest of the year. The main activity was the use of the Radio Frequency Identification (RFID) technology to trace pebbles within specific time intervals (4, 24, and 48 h after the injection). In-situ (GPS) and remote sensing (UAV) surveys were used to monitor the evolution of beach morphologies and tracer movement during the time frame of the experiment. A complete sedimentological analysis of the pebbles used as tracers was made for analysis of transport in terms of the parameters such as size, shape, and weight. The grain-size of the beach along three selected cross-shore transects was also analyzed as an additional control of variations on the backshore.

3.1. Tracing technique

The tracing technique exploits RFID technology to localize and identify individual pebbles. Passive Low Frequency (LF) RFID was identified as the ideal technology for this experiment. Previous research demonstrated that 125 kHz RFID systems can reach up to 60 cm even in seawater (Benelli et al., 2009). Moreover, passive tags do not require battery replacement and their lifetime is virtually infinite. This research used 125 kHz passive cylindrical glass tags of 4 mm diameter, 33.5 mm length and less than 2 g weight (Benelli et al., 2012), which were inserted into holes drilled in the pebbles. For locating and identification, two LF RFID readers were employed: one for the foreshore and the underwater beach, and another for the backshore. The underwater reader was customized to provide IP 68 protection allowing it to operate underwater at depths up to 3 m by placing it inside an IP 68 plastic box, perforated for power and data cables. Each reader was moved across the study area like a metal detector, detecting the tagged pebbles up to 50 cm away, either underwater or buried beneath other pebbles, and recording the unique ID code stored in the tag (Fig. 3a).

3.2. The experiment framework

The pebbles were collected randomly from the surface of the backshore to preserve a natural statistical distribution in terms of shape and weight. The only constraint was the size: the intermediate axis could not be shorter than 40 mm to fit the 33.5 mm cylinder tag. The pebbles were drilled, and the tag was inserted in the hole, then sealed with a polyester epoxy resin as in Grottoli et al. (2015). The tracers were painted with a light gray dye (Fig. 3b): this color makes finding the marked pebbles easier during short-term experiments but does not draw the attention of passers-by, who could have picked up the pebbles and distorted the results of the experiment.

In accordance with previous tracing experiments (Bertoni et al., 2013; Grottoli et al., 2019), the tracers were injected along cross-shore transects spaced ca. 5 m from each other. For each transect, two tagged pebbles were placed on the crest of the fair-weather berm, two on the swash zone, and two on the crest of the step (Fig. 4). A total of 126 tracers were used for the experiment. To avoid immediate entraining of the pebbles due to swash action, they were accommodated on the surface of the beach within the rest of the sediments rather than merely placed on top. The position of each injected tracer was recorded by means of an RTK-DGPS (Leica GS10) with an accuracy of about 2 cm. Three recovery campaigns were carried out at 4, 24, and 48 h after the injection. This activity was performed with the readers and supported by visual observations. Visual observations were especially useful for the underwater detection of the first recovery campaign at 4 h; the recoveries at 24 and 48 h were also done by a scuba diver searching the swash zone and the step base area with the waterproof reader.

3.3. Tracer sedimentological parameters

The tracers do not affect the hydrodynamic characteristics of the pebble since the hole is just 5 mm wide and the tag weighs less than 2 g. Once the tag was inserted and sealed, each pebble was measured with a caliper and weighed with a scientific scale. Axis measurement (major, intermediate, and minor) identified the shape of the pebbles in accordance with the Zingg diagram, which defines 4 shape classes: disk, sphere, rod, and blade (Zingg, 1935). As no predetermined mass classification exists for such purposes, the tracers were arbitrarily subdivided into three distinct classes based on their initial mass: heavier

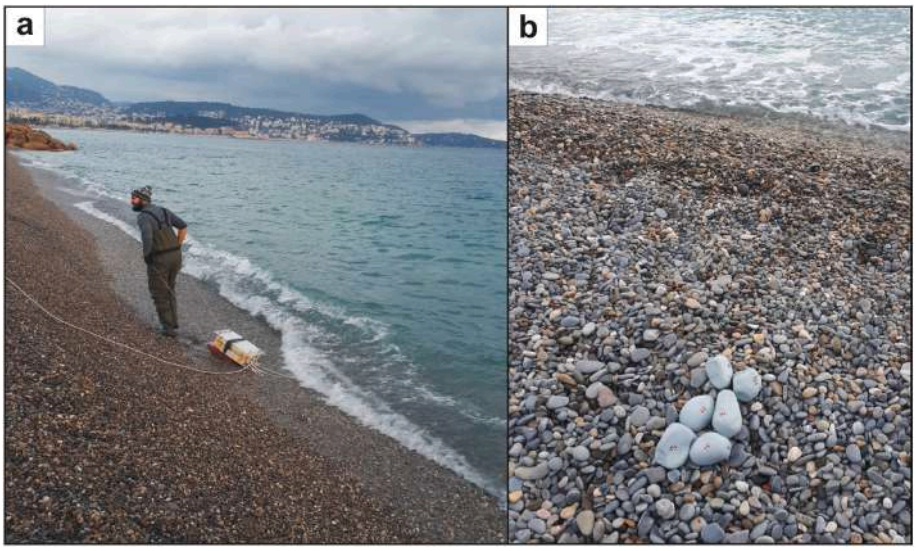

Fig. 3. The recovery campaign: the reader is dragged on the beach surface to detect the marked pebbles (a); a bunch of tracers before the injection (b).

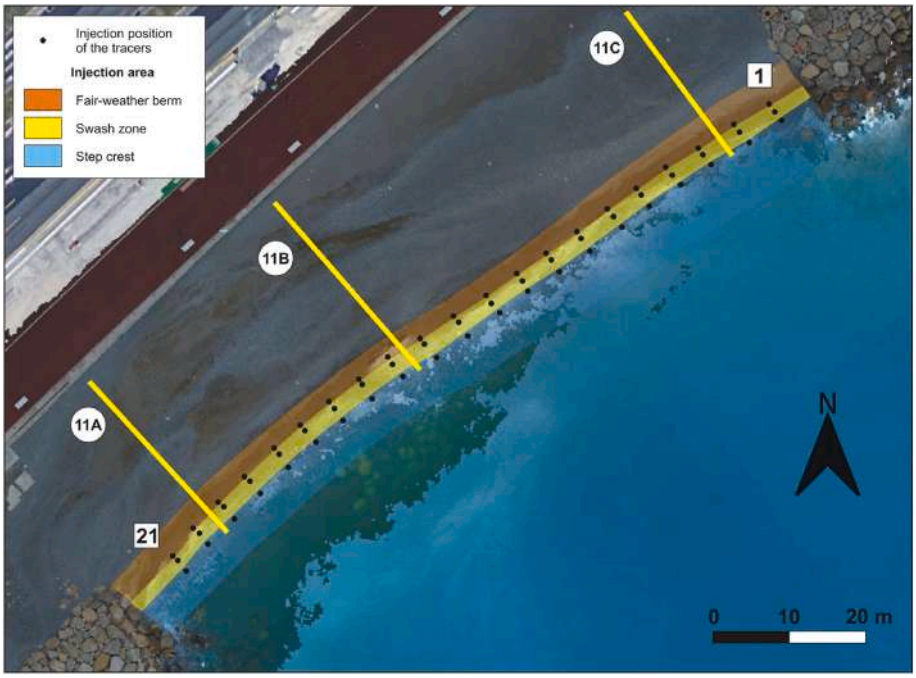

Fig. 4. The experiment setup: the black dots represent the injection position of the tracers arranged along 21 cross-shore transects (numbering starts from the northeastern end to the southwestern edge). The colored strips identify the three injection areas: fair-weather berm (orange), swash zone (yellow), step crest (blue). The thick yellow lines correspond to the cross-shore transects along which the digital grain-size analysis was carried out.

than 0.4 kg "heavy" tracers; 0.4 to 0.3 kg "medium" tracers; less than 0.3 kg, "light" tracers. Shape and mass were not considered during the injection of the pebbles, as they were placed in the initial positions randomly, regardless of these parameters.

3.4. Digital grain-size analysis

The open-source python software Digital Grain Size (pyDGS) tool was used to assess grain-size trends along the beach front. This tool was introduced in Buscombe (2013) and further developed in Cuttler et al. (2017). This technique uses wavelet analysis of pixel intensity (i.e., how 'light' or 'dark' the pixel is rather than the color hue) from images of pebbles to produce grain-size results as area-by-size, rather than the volume-by-size or mass-by-size results of other methods such as sieves and laser diffraction (Cuttler et al., 2017). The field methodology followed that conducted near Pisa, Italy (Bertoni et al., 2020). The position of the transects was selected to represent the whole beach: two towards the edges and one in the central part (Fig. 4). Though this technique is also similar to that used in Bertoni et al. (2020), a newer 4.0 version of the pyDGS software was used, which is available on a github repository (https://github.com/DigitalGrainSize/pyDGS).

A number of images on the transects included sand. Since the photo capture takes place at a distance sufficient to fit both the transect tape for reference and the 44 × 44 cm calibration square, the camera cannot resolve individual sand grains, so the results from sections of transects with bi-modality between sand and pebbles must be excluded because they either lack sufficient pebbles and/or the sand is incorrectly detected as a larger pebble.

3.5. Topographic surveys

The topography of the beach was surveyed using an Unmanned Autonomous Vehicle (UAV), specifically a DJI Phantom (DP4) equipped with a sensor camera CMOS 1''. This camera records pictures of about 20 megapixels, with a horizontal field of view of 84° to prevent distortion. The drone weighs slightly more than 1 kg, but the windless weather conditions were ideal for flying such a small UAV. Flights were completed each day during the experiment: just after the injection of the tracers (January 13th, 2020: Day 1), and before the 24- and 48-h recoveries (January 14th and 15th; Day 2 and Day 3 respectively). Each survey consisted of a single, 25-min-long flight, which was enough to patrol the entire beach; about 210 images were shot during each survey. Twelve Ground Control Points (GCP) were scattered on the backshore to improve the post-processing analysis of the dataset. These points were recorded with the RTK-DGPS for geo-referencing. The RTK-DGPS was also used for a survey just before the 4-h recovery campaign to track the morphological evolution in the first time interval of the experiment. The coordinate system used was IGNF:LAMB93. Once the Digital Elevation Models (DEM) were produced for each survey, they were processed to create Erosion/Accretion maps using the QGIS 3.16 software. Two maps were created: Day1 – Day2 and Day2 – Day3. The "Volume Calculation Tool" of the QGIS package allowed us to assess the evolution of the topography in terms of volume variations.

3.6. Model and wave parameters

The numerical simulations were run with TELEMAC, an open-source system developed by EDF R&D's Laboratoire National d'Hydraulique et Environnement (LNHE). This is an integrated modelling tool, including different simulation modules, such as TOMAWAC. TOMAWAC (TELEMAC-based Operational Model Addressing Wave Action Computation) is used to estimate the sea states by solving the balance equation of the action density directional spectrum. More details on this method can be found in Komen et al. (1994), Goda (2000), and EDF R&D (2011).

Two different grids have been used to get high resolution results at Fabron beach. The first grid covers the Nice Côte d'Azur area (global), around 4,500 m^2, with a mesh size of 250 m resulting in 93,000 nodes. The second grid covers Nice's bay (local) with a mesh size varying from 50 m offshore to 2 m in the nearshore. Then, the results of the global simulation obtained around local domain boundaries are input as boundary conditions in the local simulation. Finally, data from two buoys has been used as the boundary conditions for the global simulation. Significant wave height comes from the Côte d'Azur buoy (Latitude = 43.38, Longitude = 7.83, anchoring depth = 2,300 m), maintained by Meteo France, 60 km offshore (Fig. 1b). CANDHIS Monaco, which is a directional buoy (Latitude = 43.713, Longitude = 7.426, anchoring depth = 92 m) does record peak and mean wave direction. The Monaco buoy is located 1.6 km offshore Monaco city (Fig. 1b) and is maintained by CEREMA (Centre d'études et d'Expertise sur les Risques, l'Environnement, la Mobilité et l'Aménagement).

4. Results

4.1. Tracing experiment

For the tracing experiment, we attempted to locate all the RFID-tagged pebbles repeatedly after 4, 24, and 48 h. At each of these times, all located pebbles were left in place and we recorded their tag ID. The outcome of the tracing experiment is clearer if the area where the marked pebbles were injected is subdivided into three cross-shore zones that refer to the injection points: the fair-weather berm, the swash zone, and the step crest (Fig. 4). Therefore, the area highlighted in orange is the whole fair-weather berm from the top of the swash zone to the back of the berm crest; the yellow area corresponds to the swash zone, from the higher edge of the uprush to the step crest; the blue area extends from the step crest to the step base and the first meters of the upper shoreface. As berm and step tracers were injected on the crest of those morphological features, it is significant that the initial position of these pebbles is close to the boundary with the swash zone (yellow area); conversely, the swash zone tracers are located approximately midway through the yellow area (Fig. 4).

The recovery rate of tracers shows a peculiar trend (Table 1). After 4 h, only 70 tracers (56%) were found, but despite this, after 24 h 115 tracers (91%) were found. After 48 h the number of tracers recovered was only 18 (14%).

Only 12 of the tagged pebbles (10%) were detected in all three stages: at 4, 24, and 48 h. Three of the tracers (2%) were never found at all. The bulk of the tracers was recovered twice (59 pebbles, or 47%), while 52 just once (41%). Regarding the injection position, the recovery rates are in accordance with the general trend (Table 1). After only 4 h they were quite low especially for swash zone and step crest tracers (48% and 50% respectively), while it reached 69% for the pebbles released on the fair-weather berm. After 24 h, the recovery rates spiked up to 95% for fair-weather berm tracers; the rates were very high also for the pebbles injected in the other two zones (90% for swash tracers and 88% for the step crest). The recovery recorded the minimum values after 48 h, when the detected fair-weather berm tracers were just 24%, and hardly 10% for swash zone and step crest pebbles. The system can detect the marked pebbles within 0.5 m of the antenna. However, some tracers were only detected by the antenna and were not visually spotted. Thus, all pebbles detected within 0.5 m of their initial position were considered not to have undergone a significant displacement for the purposes of this experiment. The number of tracers that moved more than 0.5 m increased over time, starting from 79% after 4 h, getting to 90% after 24 h and reaching 100% after 48 h (Table 1). While the tracers originally injected on the fair-weather berm followed this trend (52%, 75%, and 100%), those initially placed on the step crest and in the swash zone immediately showed higher rates of transport: they reached 95% and 100% after 4 h already.

In terms of displacement (Tab. SM1), the tracers showed a clear tendency to move away from the original position, which is also why we failed to detect many pebbles (44%) after the initial 4 h of the experiment as they might have already been buried or moved to a depth out of reach of the equipment. The average total displacement increased over time, starting from 3 m after 4 h, reaching 4.2 m and eventually 25.1 m after 24 and 48 h respectively (Table 2). Looking into the three injection zones separately, the average displacement after 4 and 24 h is similar for the pebbles injected on the fair-weather berm and the step crest (2.5 and 3.7 m after 4 h, and 3.1 m both after 24 h). The similarity is even higher if an outlier pebble that moved over 30 m (#46) after 4 h is excluded: 2.5 m on the berm and 2.3 m on the step, instead of 3.7 m. Aside from that, the values in the swash zone were already higher than in the other two zones: the tracers injected there showed an average displacement of 3.1 m and 6.3 m after 4 and 24 h respectively. Highest displacements are reached after 48 h, and only three pebbles did not move over 10 m (Table 2).

The recovery zone is as important as the recovery rates and the displacement magnitudes to define potential transport trends at Fabron beach in the two days of the experiment. Already 4 h after the injection the pebbles show a tendency to move toward the step crest, as 74% of the marked pebbles were detected there (Table 3). This becomes more pronounced after 24 and 48 h (87% and 94% respectively): the 24 h value is particularly significant because it is calculated from 115 detected pebbles, as opposed to just 18 in the last recovery campaign.

Combining all three recoveries, 83% of the tracers were detected on the step crest, 12% on the fair-weather berm, and just 5% on the swash zone. Based on the transport patterns, the displacement of the tracers down the beachface is already clear after 4 h (Fig. 5a): among the detected pebbles, the large majority of those injected on the fair-weather berm and on the swash zone slid toward the step.

Just one of the tracers found back on top of the fair-weather berm

Table 1
Number of detected tracers and associated recovery rates 4, 24, and 48 h after the injection. The table also shows the number of tracers that moved more than 0.5 m from the injection position.

	Recovery rates						Displacement >0.5 m					
Injection position	4 h		24 h		48 h		4 h		24 h		48 h	
Fair-weather berm	29	69%	40	95%	10	24%	15	52%	30	75%	10	100%
Swash zone	20	48%	38	90%	4	10%	20	100%	38	100%	4	100%
Step crest	21	50%	37	88%	4	10%	20	95%	35	95%	4	100%
Total	70	56%	115	91%	18	14%	55	79%	103	90%	18	100%

Table 2
Average displacement (m) of the tracers sorted by the three injection zones. Maximum and minimum displacements are also presented.

	4 h	24 h	48 h
Fair-weather berm	2.5	3.1	28.3
Swash zone	3.1	6.3	26.8
Step crest	3.7	3.1	15.6
Average total displacement	3	4.2	25.1
Max displacement (fair-weather berm)	14.7	5.8	63.1
Min displacement (fair-weather berm)	0	0	8.8
Max displacement (swash zone)	4.9	68.4	52.4
Min displacement (swash zone)	1.1	0.9	6.1
Max displacement (step crest)	30.1	11.3	29
Min displacement (step crest)	0	0	9.3

Table 3
Tracer recovery rates sorted by the detection zone. The "Total" column corresponds to the cumulative number of pebble detections on each zone.

	4 h	24 h	48 h	Total
Fair-weather berm	15 (22%)	9 (8%)	1 (6%)	25 (12%)
Swash zone	3 (4%)	6 (5%)	0 (0%)	9 (5%)
Step crest	52 (74%)	100 (87%)	17 (94%)	169 (83%)
Total number of detection	70	115	18	203

came from elsewhere, while the remainder did not move significantly from their injection position. The three pebbles retrieved in the swash zone all came down from the fair-weather berm (Fig. 5a). No clear-cut trend in terms of longshore transport can be identified, even though the tracers that rolled down from the fair-weather berm and the swash zone manifested a southwest shift. A preferential longshore movement is barely discernible during the second time interval as the tracers injected at the southwest end of the beach tended to move toward the northeast (Fig. 5b). The transport patterns in the northeast end are not different from that recorded after the first 4 h, which was characterized by a widespread prevalence of cross-shore movement. Likewise, the tracers recovered on the top of the fair-weather berm did not undergo transport at all, except one which came from the swash zone in the central sector of the beach. The pattern changed dramatically after the 48 h recovery (Fig. 5c): the longshore component clearly prevailed over the cross-shore, with all the tracers moving toward the northeast end of the beach. The only pebble found back on the berm was originally injected on the fair-weather berm along a transect located in the central sector of the beach. This tracer experienced the most displacement (63.1 m).

4.2. Shape and mass effects on transport

The shape of the tracers was plotted on a Zingg diagram (1935), which shows the four fundamental shapes of natural objects: disk, sphere, blade, and rod. As the pebbles were sampled randomly, this is likely representative of all the Fabron beach pebbles of that size range. The resulting Zingg diagram documents that disks and spheres are the prevailing shapes with 39% and 34% respectively while rods are 20%; blades are just 7% (Fig. 6). The distribution is typical of a natural setting.

Unsurprisingly, the recovery percentage of the tracers sorted by shape follows the general trend: just average after 4 h, very high after 24 h, and low after 48 h (Table 4). Four hours after the injection the less frequent classes (rods and blades; 36% and 33%) were recovered significantly less than the other two classes (disks and spheres; 71% and 53%). The recovery of disk-shaped pebbles is particularly high after 4 h, and it is the higher than any other class in the first time interval; it is also above the general recovery rate (56%). The recovery rate increases after the second campaign, reaching values close or over 90% for each shape class in accordance with the general trend (91%). Disk and rod recoveries are identical to that trend (92% each), while spheres are slightly below (88%); blades show a perfect 100% (Table 4).

After 48 h sphere- and blade-shaped tracers show the highest recovery rates (21% and 22% respectively), both over that of the general trend (14%); disks do not deviate from it (12%), while rods are well below (4%). Some peculiar features emerge analyzing the transport patterns of the tracers sorted by the shape (Fig. 7 and Table 4). The preferential seaward shift of pebbles is clearly confirmed for each shape class, as well as the scarce number of tracers found back on the swash zone. These patterns also work if one analyzes the three recovery campaigns separately, with just one exception: one blade-shaped pebble was detected on the swash zone after 24 h, whereas no other blade was found back on the fair-weather berm during the same recovery campaign (Fig. 7 and Table 4). The statistical significance is negligible however. The only trend pebble shape shows is that disk-shaped tracers display higher recovery rates on the fair-weather berm during each campaign. The only pebble recovered on the fair-weather berm after 48 h was a disk. In terms of displacement vs. pebble shape (Table 5) shifting increases over time. Spheres and rods are characterized by average values that resemble the general trend during each time interval. Blades differ more, but the sample (just 9 tracers) is not big enough to be dependable.

However, disk-shaped pebbles show values that exceed the general trend after the second and third recovery campaigns; the average displacement after 48 h is especially high: 34.7% as opposed to 25.1%. Sorting by the shape does not highlight any peculiar tendency in terms of the rate of tracers that moved over 0.5 m (Table 5). All shape classes show a high number of pebbles moving more than 0.5 m right after 4 h (over 70%); this number increases after the subsequent campaigns to over 80% (24 h) and 100% (48 h).

Displacement sorted by mass does not highlight any trend (Fig. 8). After 4 h, tracers that moved within 1 m from the injection site were well balanced between light, medium, and heavy pebbles (less than 20%); likewise, tracers of the three mass classes that moved more than 1 m were all close to 40%; the maximum range is among the tracers that got lost: undetected light pebbles were 55%, medium pebbles just less than 40%, and heavy pebbles about 45%. The next two recovery campaigns show an even distribution among the three mass classes in all the parameters investigated (Fig. 8).

4.3. Digital grain-size analysis

The grain-size characterization of the surface sediments constituting Fabron beach was provided by the Digital Grain-size analysis technique. About 200 pictures were shot along the three transects (Fig. 4). The photo set consists of 69 pictures on Transect 11C, 51 on Transect 11A, and 55 on Transect 11B. The pattern of grain-size variation along each

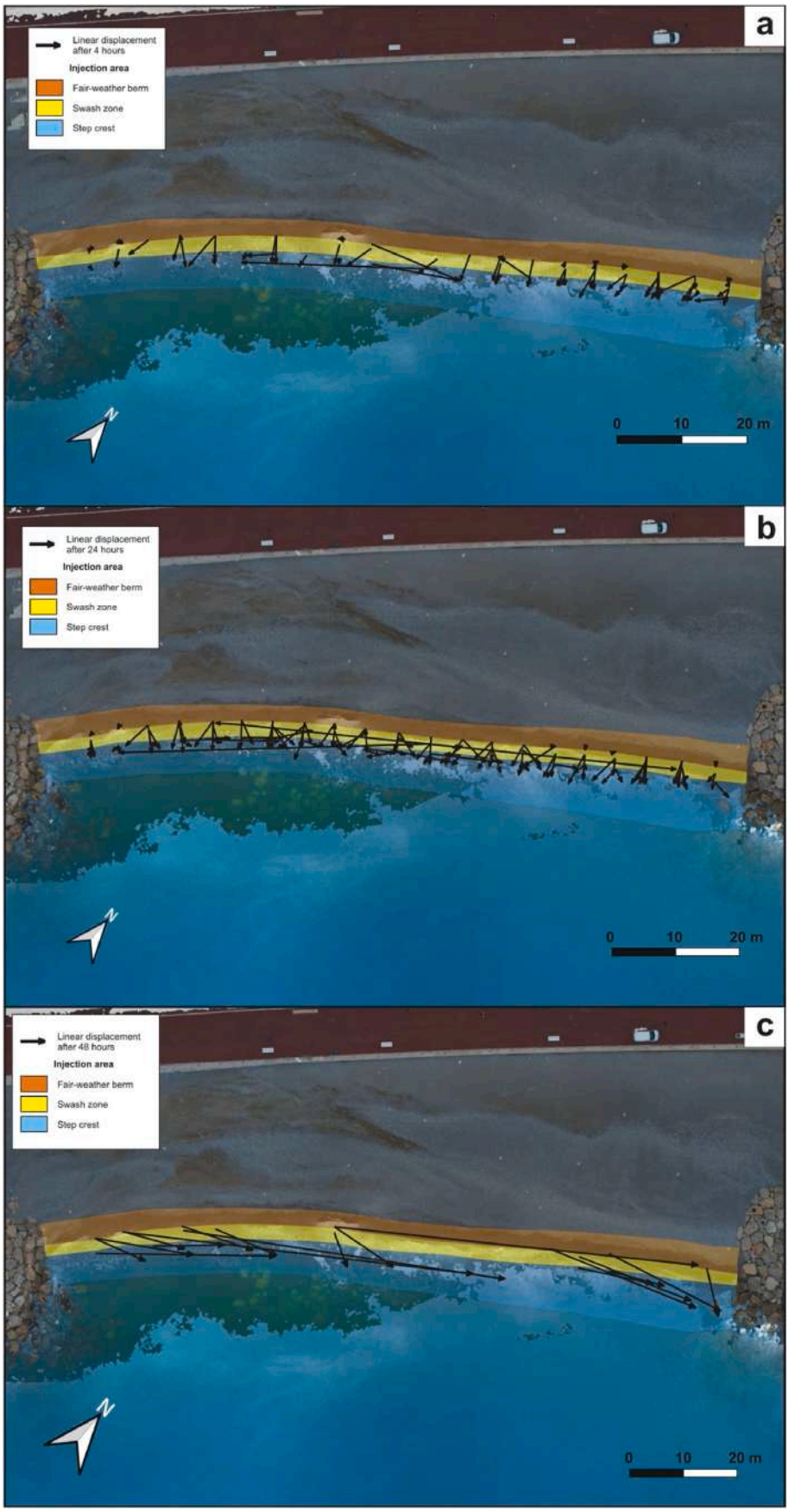

Fig. 5. Transport trajectories of the detected tracers during the first time interval (4 h, a), the second time interval (24 h, b), and the third time interval (48 h, c).

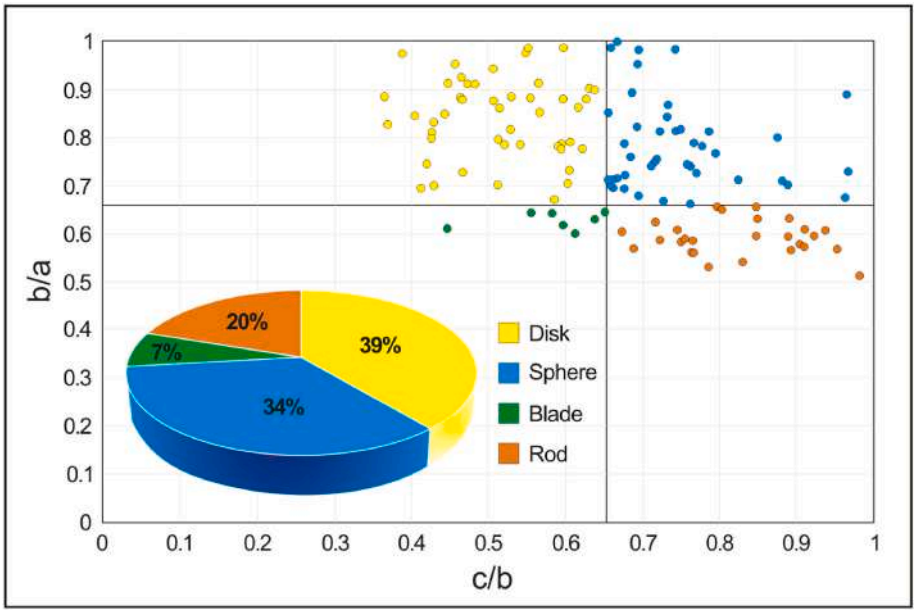

Fig. 6. Shape characterization of the 126 tracers in accordance with the Zingg diagram. The tracers were randomly sampled from the backshore.

Table 4
Recovery rates sorted by the shape of the tracers.

Disk	Injected	Recovered	Fair-weather Berm	Swash Zone	Step Crest
Injection	49	–	19	14	16
4 h	–	35 (71%)	9 (25%)	2 (6%)	24 (69%)
24 h	–	45 (92%)	5 (11%)	3 (7%)	37 (82%)
48 h	–	6 (12%)	1 (17%)	0 (0%)	5 (83%)
Sphere	**Injected**	**Recovered**	**Fair-weather Berm**	**Swash Zone**	**Step Crest**
Injection	43	–	14	18	11
4 h	–	23 (53%)	5 (22%)	1 (4%)	17 (74%)
24 h	–	38 (88%)	2 (5%)	1 (3%)	35 (92%)
48 h	–	9 (21%)	0 (0%)	0 (0%)	9 (100%)
Blade	**Injected**	**Recovered**	**Fair-weather Berm**	**Swash Zone**	**Step Crest**
Injection	9	–	2	3	4
4 h	–	3 (33%)	0 (0%)	0 (0%)	3 (100%)
24 h	–	9 (100%)	0 (0%)	1 (11%)	8 (89%)
48 h	–	2 (22%)	0 (0%)	0 (0%)	2 (100%)
Rod	**Injected**	**Recovered**	**Fair-weather Berm**	**Swash Zone**	**Step Crest**
Injection	25	–	7	7	11
4 h	–	9 (36%)	1 (11%)	0 (0%)	8 (89%)
24 h	–	23 (92%)	2 (9%)	1 (4%)	20 (87%)
48 h	–	1 (4%)	0 (0%)	0 (0%)	1 (100%)

transect is roughly similar (Fig. 9): sediments are coarse at the toe of the seawall at the back of the backshore (mean diameter of ca. 31 mm), then get coarser in the central portion of the profile at the landward toe of the storm berm (ca. 35 mm). The seaward side of the storm berm is characterized by finer pebbles on transects 11A and 11B (ca. 32 mm), while the grain-size is coarser on Transect 11C in that same spot (ca. 34 mm). The portion close to the fair-weather berm and the coastline is generally finer along each profile (ca. 31 mm). The crest of the storm berm is the only part of the profile that differs among the three transects: 11A shows a mean diameter of 32 mm, 11C is coarser (ca. 34 mm); 11B presents a small but not negligible sand spot. All in all, Transect 11C is coarser than the other two: it is not just for the two clusters of pebbles with grain-size coarser than 34 mm at both edges of the storm berm, also there are no sand accumulations along this profile, which stand out in the other two transects (Fig. 9).

4.4. Morphological evolution

Three drone surveys were carried out in the morning of each day to define the morphological characteristics of the backshore during the time frame of the experiment. The data have been processed to obtain accretion/erosion maps that clearly shows the evolution of the topography during the intervals between each recovery campaign (Fig. 10).

The first map shows the surveys performed at injection time and before the 24 h campaign (Fig. 10a): no apparent major variation occurred during the first 24 h; the northeastern end presents areas where the sediments were displaced and shifted elsewhere, causing volume loss. The map documents the erosion of the crest of the fair-weather berm in the northern edge of the beach. The erosion increased over time, as it spread throughout the compartment after 48 h (Fig. 10b): the fair-weather berm was wiped out during the following 24 h, except at the northern end of the beach, where significant accretion is reported. However, small but rather continuous accretion strips are identified right behind the large erosion band. In this second interval, the only sector of the beach that underwent erosion at the crest of the fair-weather berm is toward the northern end, just before the accretion area. The volume calculation was performed excluding the backshore area as there were no appreciable variations there, except for minor changes due to the passage of excavators heading to beach compartments where maintenance work was ongoing. The results confirm the documented trend as the difference between Day 1 and Day 3 is about $-16\ m^3$.

An additional topographic survey was conducted along five cross-shore transects 4 h after the injection, and its results were plotted against the data extracted from the DEMs along the same profiles to emphasize the topographic variations of the beach during the time frame of the experiment (Fig. 11).

Firstly, the transects confirm that the width of the compartment is not uniform throughout: the southern edge is about 26 m wide, whereas the northern one is 35 m wide. In accordance with the accretion/erosion maps (Fig. 10), the profiles do not show any modification on the backshore up to the crest of the fair-weather berm from injection time to the 48-h recovery. However, the seaward side of the fair-weather berm displays small but crucial variations: during the first 4 h of the

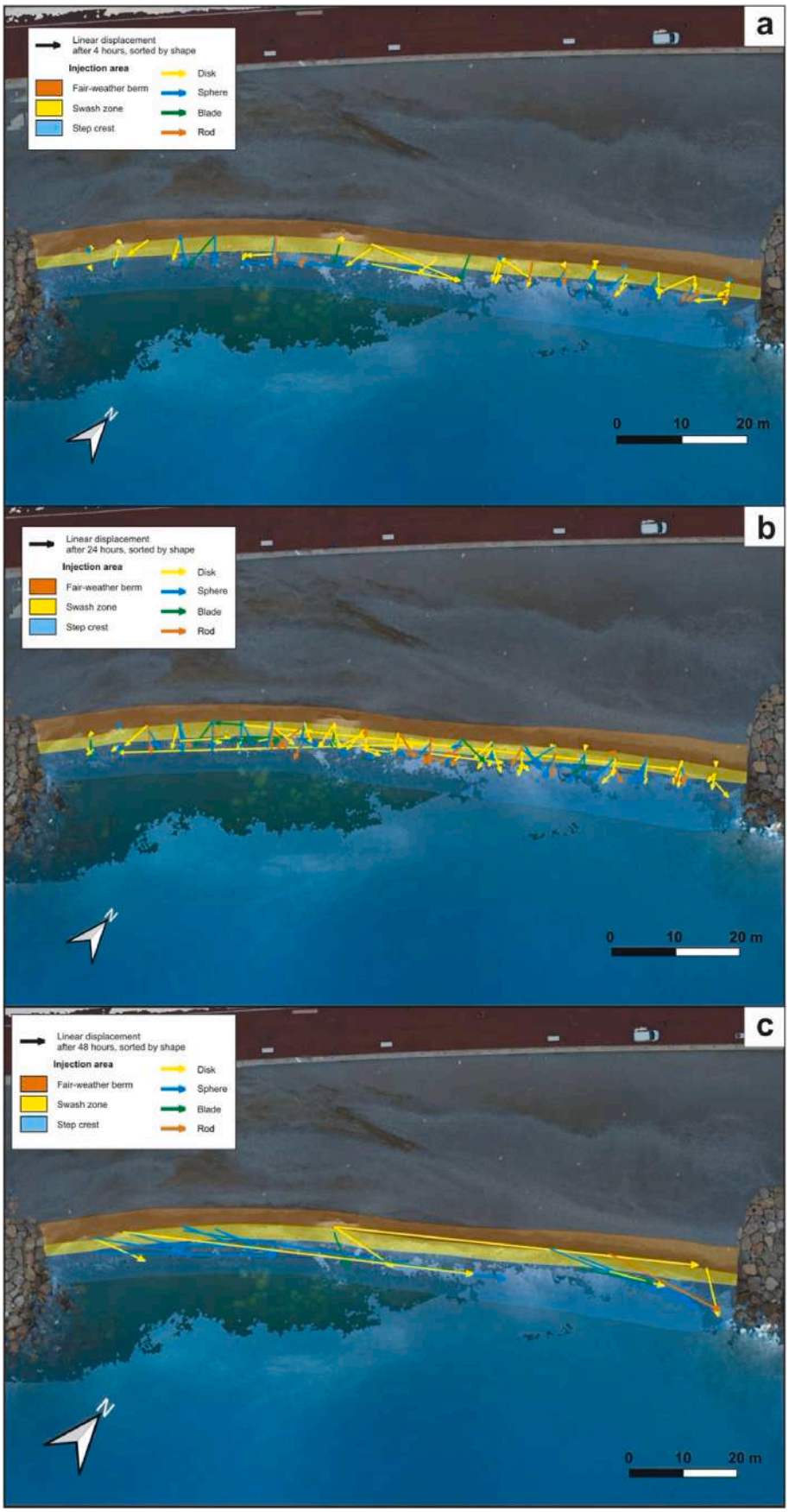

Fig. 7. Transport trajectories of the detected tracers during the first time interval (4 h, a), the second time interval (24 h, b), and the third time interval (48 h, c) sorted by the shape of the pebbles (yellow: disks; blue: spheres; green: blades; orange: rods).

Table 5
Tracer average displacement and recovery rates of pebbles that moved more than 0.5 m sorted by the shape.

		4 h	24 h	48 h
Disk	Average displ.	2.8	5.2	34.7
	Recovered >0.5 m	26	37	6
	Recovered >0.5 m (%)	74	82	100
Sphere	Average displ.	3.6	3.4	22.8
	Recovered >0.5 m	19	36	9
	Recovered >0.5 m (%)	83	95	100
Blade	Average displ.	4.5	4.3	9.2
	Recovered >0.5 m	3	8	2
	Recovered >0.5 m (%)	100	89	100
Rod	Average displ.	2.1	3.4	20.3
	Recovered >0.5 m	7	22	1
	Recovered >0.5 m (%)	78	96	100

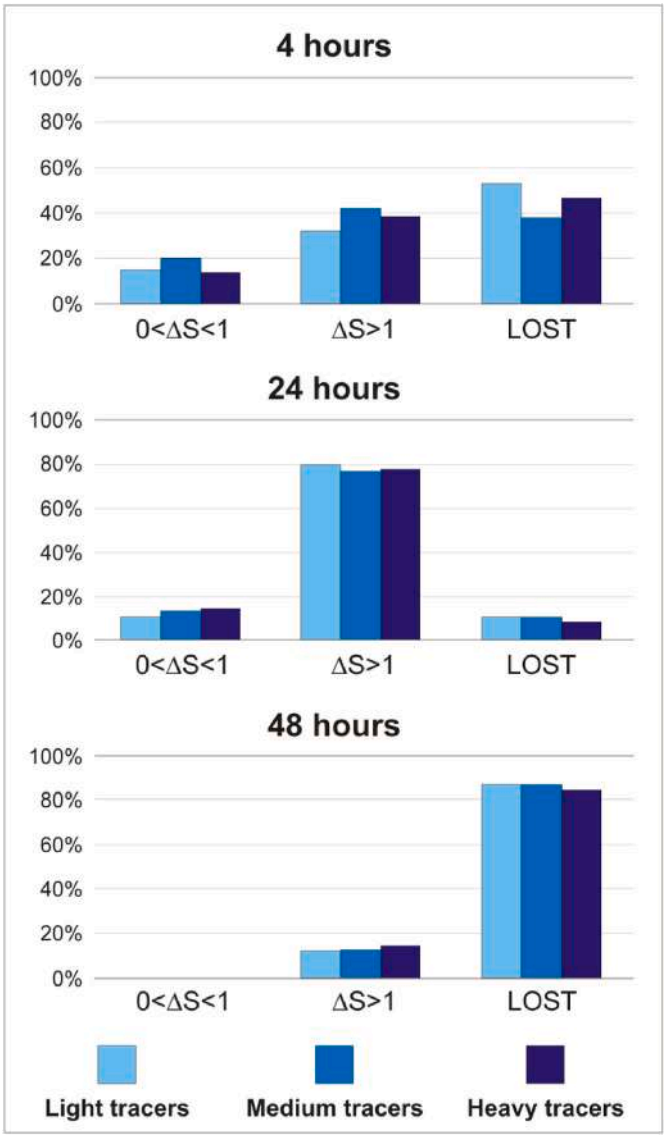

Fig. 8. Distributions of the tracers after all three recovery campaigns sorted by the initial mass (light, medium, and heavy tracers). The distributions of each mass class are further analyzed according to tracer offset length from the injection position ($1 < \Delta S < 1$ m and $\Delta S > 1$ m), and if the tracers went undetected (LOST).

experiment each profile shows consistent signs of erosion (Fig. 11). Then the initial configuration of the fair-weather berm is restored during the next 24 h, as the Injection and 24-h profiles are almost identical. The 48-h profile shows major differences, as transects 1 to 4 are characterized by a significant sediment loss; only transect 5 presents accretion (Fig. 11).

4.5. *Wave parameters and simulation model*

The identification of wave characteristics during the study was paramount to interpret the outcome of the tracing experiment. Wave data recorded by the CANDHIS Monaco buoy showed that the significant wave height was quite low (below 0.3 m) until the afternoon of the second day, then increased by about 0.5 m during the rest of the time frame (Fig. 12a). Mean wave direction was not constant. Incoming waves approached the coast from the southeast in the early stage of the experiment; wave direction turned to south-southeast and then south in the afternoon of the first day, and did not change again (Fig. 12b).

The tide record showed three high-tide peaks at the time of the injection and the 24- and 48-h recovery campaigns; two minor oscillations occurred with an offset of 12 h from the injection and the 24-h survey (Fig. 12a). Wave records from the Monaco buoy allow a direct comparison with the parameters provided by the wave simulation model. The datasets overlap well, especially the direction parameter; the trend of the simulated wave height matches the recorded data until the morning of the second day: thereafter it exceeds the recorded values by 0.2–0.3 m (Fig. 12a and b). Based on this comparison, the accuracy of the global simulation is quite high, and the outcome is assumed to be reliable.

The simulation model helped reconstructing parameters such as wave height and direction during the time frame of the experiment at Fabron beach. The simulation confirmed that incoming waves came from the southeast at the time of tracer injection and were characterized by a height of just 0.2 m (Fig. 13a). Wave height decreased over the next 4 h, reaching about 0.1 m at the time of the first recovery campaign in the afternoon of the first day; wave direction did not change (Fig. 13b).

As documented by the recorded data, the major variations occurred over night. Despite a slight increase of the wave height (0.3 m offshore of Fabron beach, and around 0.2 m in the nearshore), the wave direction shifted to the south-southeast on the afternoon of Day 1; by the time of the second recovery campaign at 24 h, the shift is still not complete (Fig. 13c). During the last interval at the 48 h recovery campaign, the simulation shows the change in wave conditions: wave height spiked to 0.5–0.6 offshore, while it was around 0.4 m at the Fabron beach nearshore zone; wave direction continued to shift westward until reaching due south (Fig. 13d).

5. Discussion

The most interesting result of this tracing experiment is the uncharacteristic transport pattern compared to previous short-term investigations involving the use of marked pebbles, which documented a progressive decrease of detected tracers as time went by (Bertoni et al., 2013; Grottoli et al., 2015, 2019). Here, detection was just 56% after 4 h, skyrocketed to 91% after 24 h, and eventually fell to 14% after 48 h (Table 1). However, Dickson et al. (2011) also reported very low detection rates after two days, but they increased to approximately 50% in subsequent recoveries. They explained such a pattern with the occurrence of a storm during the second day of the experiment, which did not occur during the time frame of the Nice's test. The roller-coaster pattern at Fabron beach reflects the high mobility of the tracers, as they are characterized by significant displacement even after 4 h (Table 3). While the immediate tendency to move away from their injection spot justifies this unexpected loss, it does not explain why many undetected pebbles reappeared during the second recovery campaign, as the average displacement increased after each survey. The general pattern

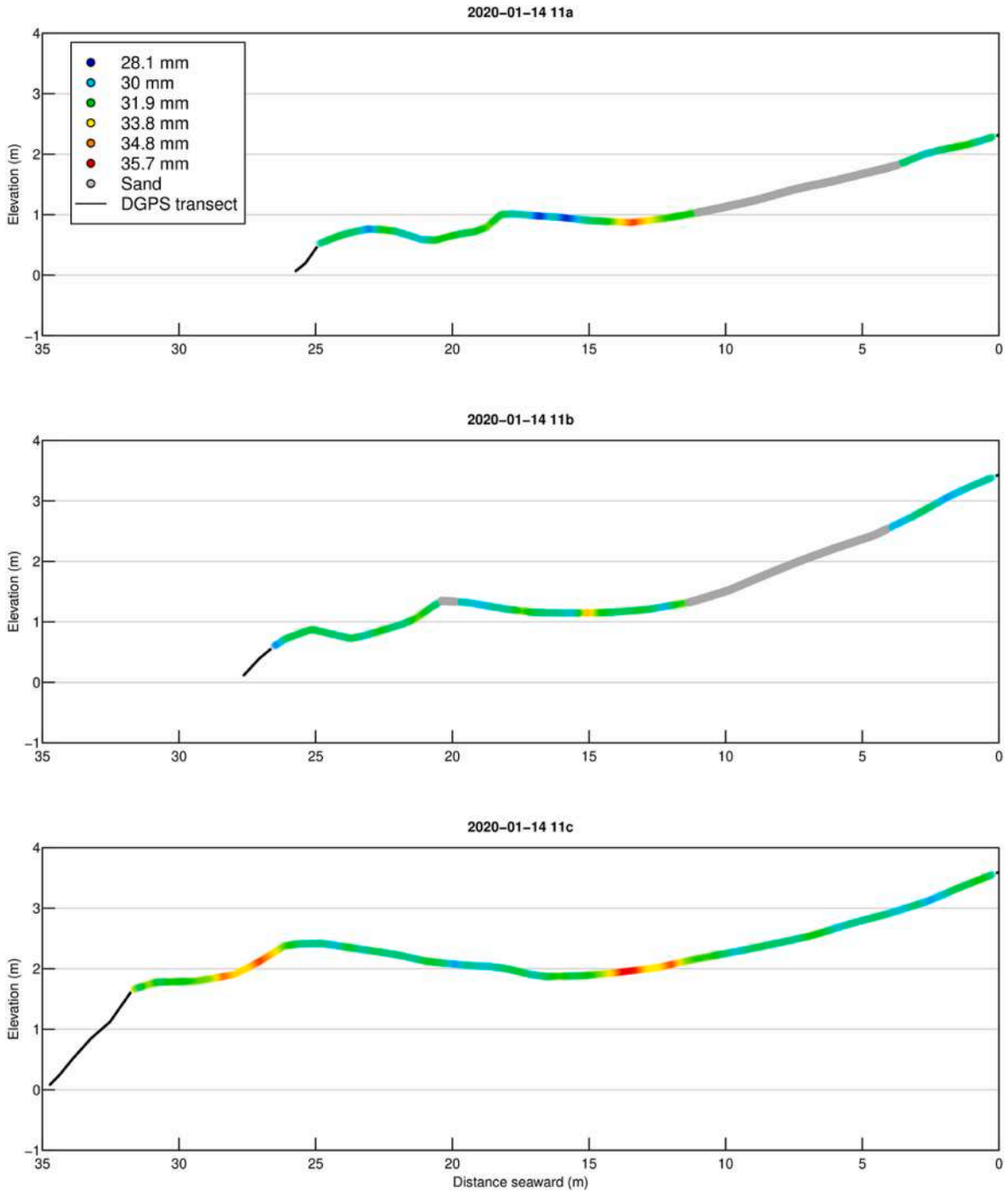

Fig. 9. Grain-size characterization of the backshore at Fabron beach along the three reference cross-shore transects: 11A, 11B, and 11C.

does not depend on the injection position of the tracers: the experimental design was identical to past experiments (Fig. 4), and pebble recovery rates sorted by the original position followed the total rates. Sorting the detection rates according to the recovery zone does not show any relationship, as the tracers tend to roll down the beachface in a cross-shore direction, amassing on the step crest eventually (Fig. 5): this pattern was already reported, especially under low wave conditions (Miller et al., 2011; Bertoni et al., 2013; Grottoli et al., 2015) and seasonally (Casamayor et al., 2022). Likewise, there is no hint that the longshore transport might affect the general pattern, as the clear northeastward movement of the tracers only surfaced during the last 24 h: the first two recoveries do not show any obvious longshore trend, as the cross-shore movement is prevalent (Fig. 5). The sedimentological parameters such as shape and mass are not responsible for the reported general pattern as they follow the trend accordingly (Table 5; Figs. 7 and 8). Therefore, if none of the aspects related to experimental design and tracer displacement can explain the documented pattern, the morphological evolution of the beach must be taken into consideration (Fig. 11). The topography of the foreshore at injection time and after 24 h is similar, but such an equilibrium is just apparent. As a matter of fact, the 4-h profile clearly demonstrates that the fair-weather berm went through a destruction/rebuilding phase during the first 24 h of the experiment. Tidal data show that tracer injection was performed at high tide (Figs. 12 and 13); despite the wave height being just less than 0.4 m during the first stage of the experiment, the water could reach the highest part of the swash zone, inducing scouring processes at the

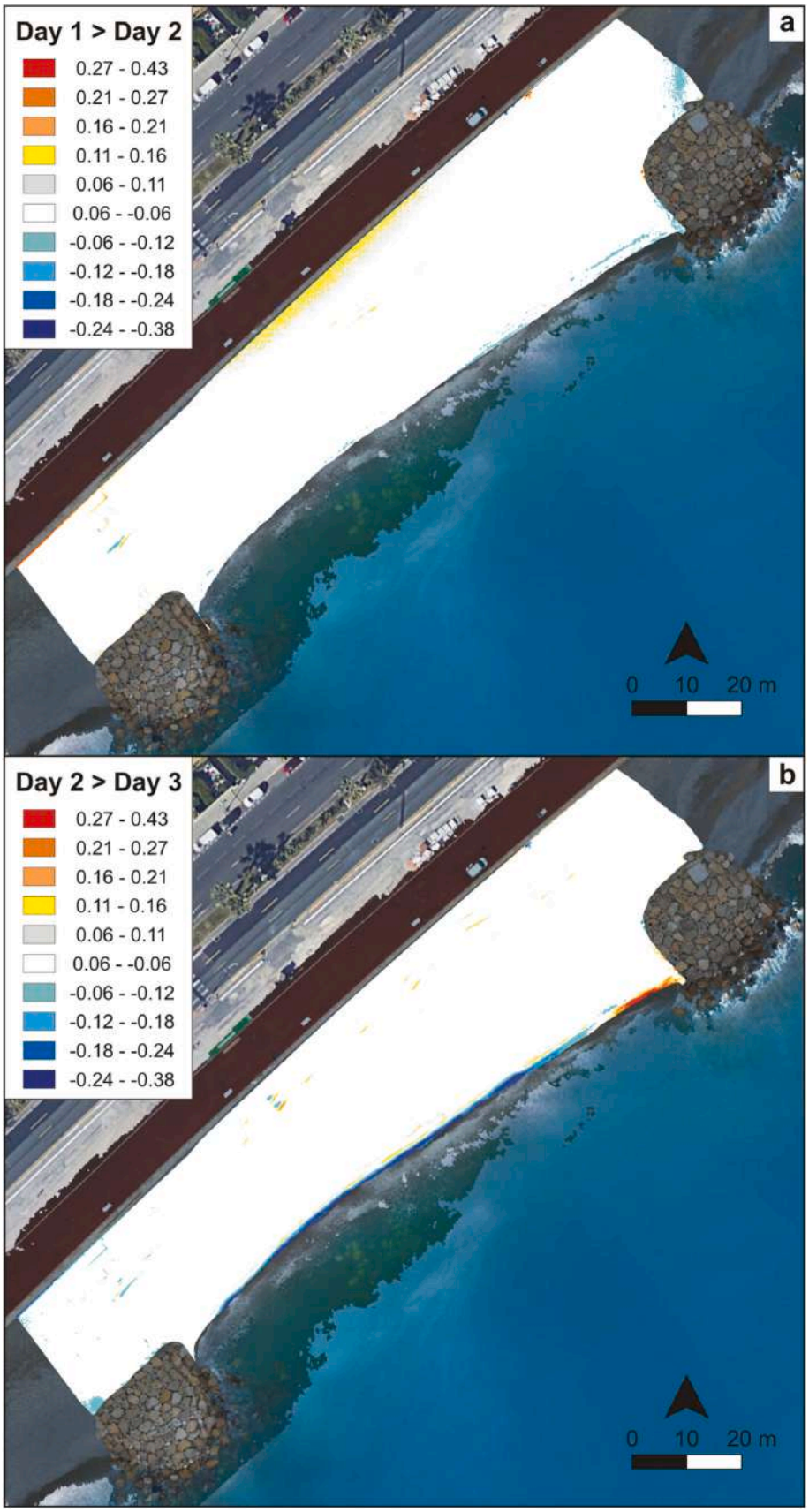

Fig. 10. Accretion/erosion maps resulting from the drone surveys (values are expressed in m^3). Difference between Day 1 and Day 2 (a) and difference between Day 2 and Day 3 (b).

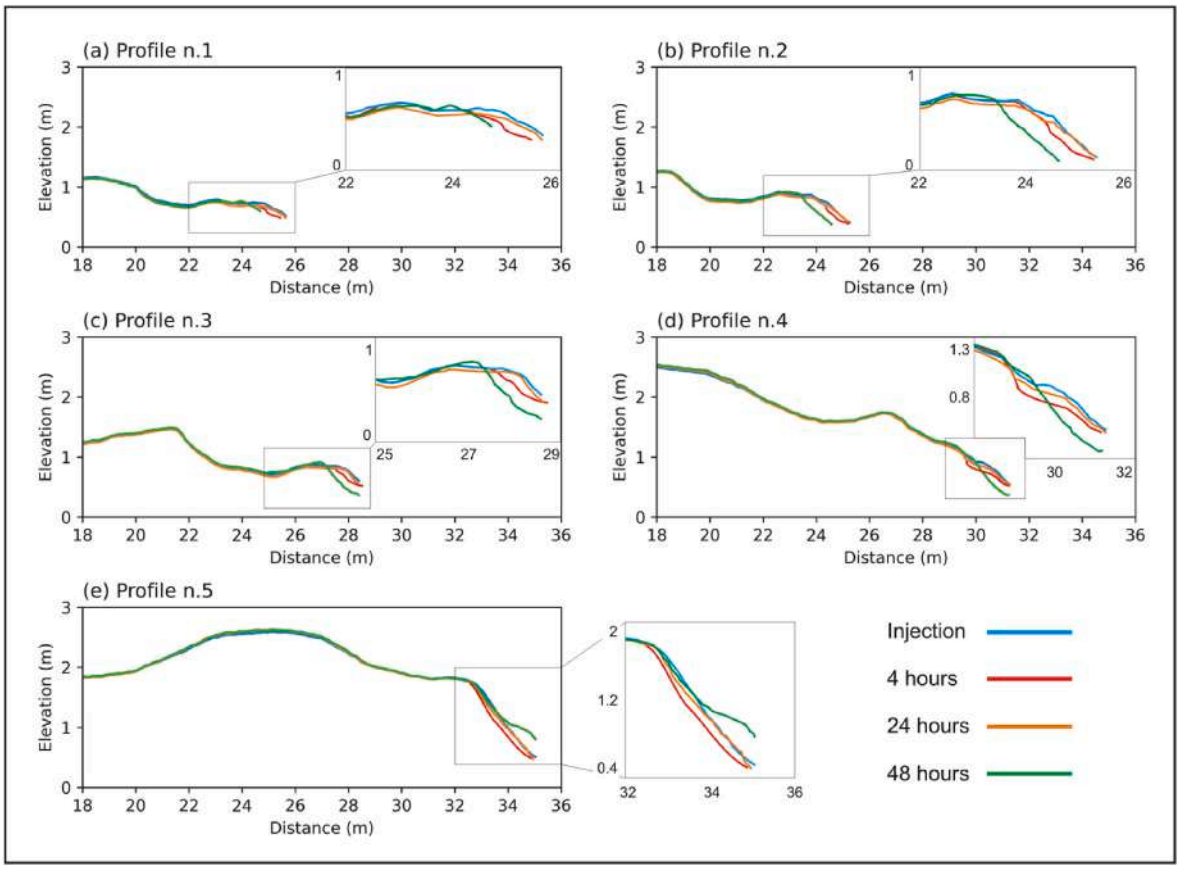

Fig. 11. Topographic variations along five cross-shore transects during the time frame of the experiment. The panels do not show the higher part of the backshore to better appreciate the differences between the surveys, which only occurred next to the shoreline (additional zoom-ins are provided for the last 4 m of each profile).

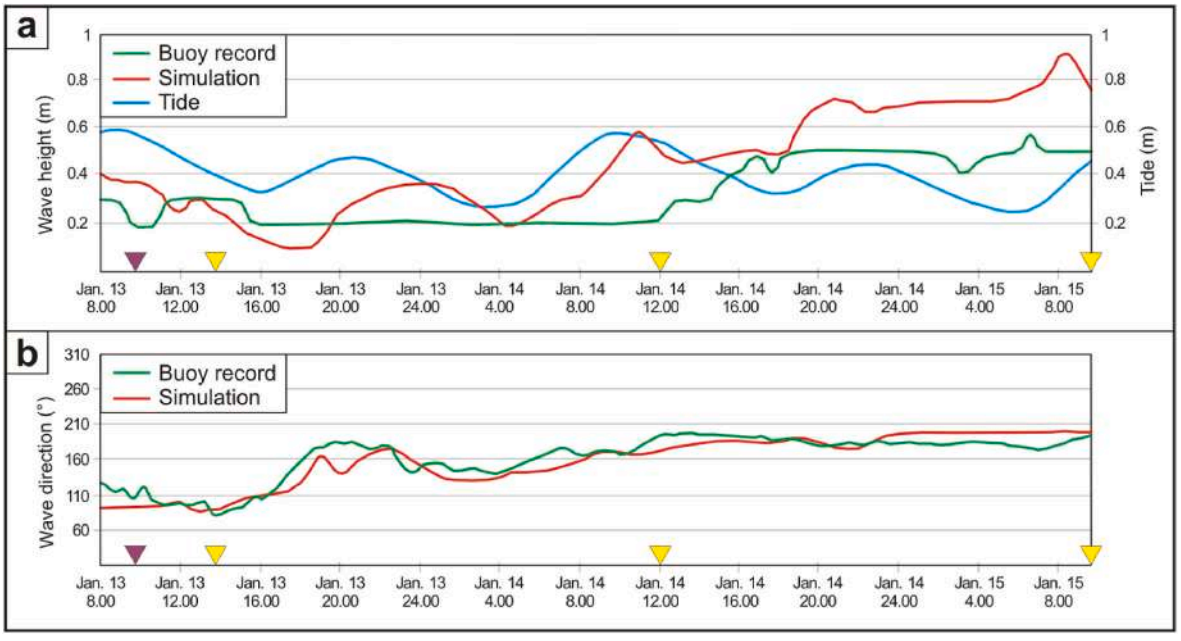

Fig. 12. Wave parameters during the time frame of the experiment. Comparison between the data recorded by the CANDHIS Monaco buoy (green lines) and those provided by the simulation model (red lines). The parameters taken into consideration are the significant wave height (a) and the wave direction (b). The blue line in panel a represents the tide oscillations during the experiment. The purple triangle marks the tracer injection time, the yellow triangles the three recovery campaigns (4, 24, and 48 h).

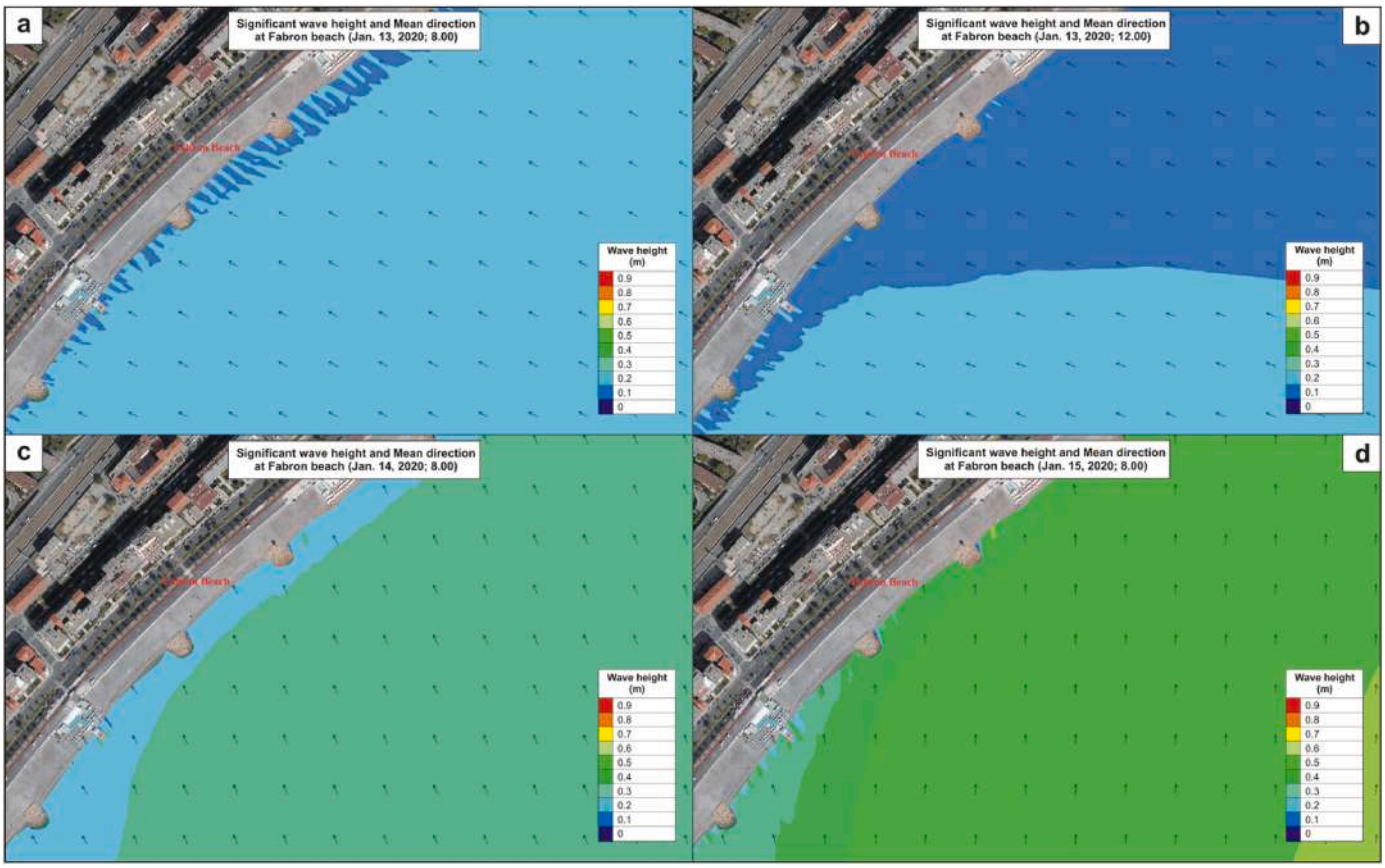

Fig. 13. Wave height and direction resulting from the simulation models at 4 different times during the experiment: tracer injection (a), recovery after 4 h (b), recovery after 24 h (c), and recovery after 48 h (d).

fair-weather berm base. This process increased the instability of the crest of the fair-weather berm: visual observations confirmed that pebbles moved downslope from the crest to the lower part of the swash zone. In this way, many berm- and swash-zone-injected tracers were quickly removed from their initial spots, ending up over the step crest in an area beyond the reach of the antenna. Furthermore, some of the undetected tracers might have been buried under the pebbles coming over from the demolition of the fair-weather berm, which prevented any chance of visual detection as well. Clearly, the downslope movement of the pebbles was also favored by the considerable slope of the beach, which reaches an average value of 0.38 in the swash zone.

In the next stage, wave height decreased to less than 0.2 m, which likely prevented reworking taking place. In the early morning of Day 2 wave height of about 0.6 m coincided with the rising tide: this combination of processes may be responsible for scraping the surface of the swash-zone. The pebbles that reached the step area in the first stage might have been reworked and pushed back up, reshaping the fair-weather berm to its former configuration and unearthing many tracers for easy detection during the recovery campaign at the 24 h mark. This also explains the landward cross-shore movement of some tracers. The wave height picked up during the last stage, remaining over 0.5 m until the end of the experiment, with peaks of more than 0.8 m in the morning of Day 3 (Figs. 12 and 13). Such a strengthening of the wave motion induced more invasive erosion of the fair-weather berm compared to Day 1, which led to a huge reworking of the system and to the eventual reported tracer loss (86%). The process of berm destruction/rebuilding in short timespans has already been observed on coarse-clastic beaches (e.g., Buscombe and Masselink, 2006; Russell et al., 2009) and in laboratory experiments (e.g., McCall et al., 2015; Muhajjir et al., 2019), but it is less documented especially where the backshore leans against a massive seawall: here, beach recovery is not as effective as elsewhere because strong wave reflection prevents accretion processes from occurring (Bertoni and Sarti, 2011; Grottoli et al., 2017). However, in a previous experiment carried out using the same experimental set-up, Grottoli et al. (2019) reported a different evolution of the swash zone morphology in a mixed-sand-and-gravel beach at Portonovo, as a new fair-weather berm formed in front of the one present at the beginning of the experiment. The development of this fair-weather berm acted as a barrier for the tracers that were injected on the crest, which were prevented from any kind of movement. This explains the difference in the number of berm tracers that did not experience any movement documented in the studies, as about half of the berm tracers did not move at Portonovo as opposed to less than 15% at Nice beach. Clearly, the significant difference in the slope of the nearshore between the two beaches (0.11 at Portonovo vs 0.38 at Nice, calculated in the swash zone) factors in, and it is likely responsible for the different evolution of the morphology.

Accretion processes are more common on coarse-clastic beaches where beach rotation is reported: depending on the incoming wave direction the sediments move in accordance with the drift, accumulating on either ends of the beach (Ruiz de Alegria-Arzaburu and Masselink, 2010; Karunarathna et al., 2012; Scott et al., 2016; Wiggins et al., 2020). The simulation model and the wave data highlight the presence of a shift in wave direction in the afternoon of Day 1. The SW – NE orientation of the Fabron Beach and the wave direction obtained from the model are both consistent with the actual direction of transport we found of the pebbles during the time interval between 24 and 48 h (Fig. 5). Likely, Fabron beach is subject to beach rotation processes. Topographic surveys revealed that the northeastern part of the compartment is wider than the other end, but the extent of this accumulation would be much larger if the sediments would not be able to move back to the southwestern edge during southeastern wave events. The 4- and 24-h recovery

campaigns showed no clear indication of longshore transport, despite a few tracers from the southwestern edge appeared to move to the central sector of the compartment, which is consistent with the mentioned wave shift. This means that the eastward drift is not always present under every sea-state condition. Besides, Anthony et al. (2011) stated that the littoral drift along Bay of Nice is bidirectional, depending on the incoming wave direction. As only beach drift was measured in the present study, it is not surprising.

Despite the sedimentological parameters not heavily influencing the overall recovery pattern, they contributed to some specific trends that might impact the evolution of Fabron beach. Disk-shaped tracers stood out in terms of recovery rate (Table 5): especially after 4 h, they were detected well above the total percentage (71% vs 56%). Moreover, the disk shape is most commonly found on the fair-weather berm. Lastly, disks also show the highest average displacement length among all the shapes. Combining all these elements leads to the conclusion that disk-shaped pebbles are less prone to downslope shifting than spheres, which can easily roll down the beachface. As disk-shaped pebbles are not mobilized as quickly as spheres, they have been detected more often on the fair-weather berm. However, once they are displaced, they can reach further distances just sliding over the beachface in a longshore direction. These results are in contrast with those documented from both gravel and mixed-sand-and-gravel beaches from different settings (e.g., Orford et al., 2002; Hayes et al., 2010; Grottoli et al., 2017; Grottoli et al., 2019). This might be a case of particle rejection/acceptance adapted to shape rather than size: according to Moss (1962, 1963), finer particles accommodate in the interstices between coarser particles, while coarser particles overpass the finer particles. In the same way, more regular shapes such as spheres might fit better than wider, more irregular shapes such as disks in the interstices of sediments, which would lead to higher chances of increased distance travelled by disk-shaped tracers. This occurrence might be also favored because of the irregular surface of the swash zone at Fabron beach, which is constituted by coarse sediments. Nonetheless, Grottoli et al. (2015) document such a pattern also on a sandy beachface of a mixed-sand-and-gravel beach in the Adriatic Sea, while Stark and Hay (2016) report this tendency on a higher-energy, mega-tidal beach. Conversely, sphere-shaped pebbles reach the lower part of the swash-zone soon after the injection; here, gravity contributes to the downslope movement of the tracers. Once there, they hardly move again under low wave motion (Fig. 7). While the shape parameter tells something about the transport processes, mass does not. The results do not show any mass-related tendency, as pebbles of any mass (heavy, medium, light) have similar probabilities of not undergoing transport, moving downslope, or getting lost (Fig. 8 and Tab. SM1). Thus, gravity exerts the same influence on the transport patterns of pebbles, regardless of mass. Considering that the pebbles used for tracing purposes were among the coarsest in the population – required to accommodate the cylinder tag – it implies that at Fabron beach a low wave motion is capable of moving the sediments regardless of the mass parameter.

5.1. Management considerations

A better understanding of coarse sediment transport patterns is essential to any attempt of improving the management of coarse-clastic beaches. The RIFD technique has already proven to be a reliable way to track sediments on different settings (Allan et al., 2006; Curtiss et al., 2009; Bertoni et al., 2013) and still is the best method for uniquely identifying pebbles and their transport patterns. Chronic offshore loss of sediments is the main cause of erosion along the Bay of Nice, and the insights of this tracking experiment can help manage the environmental and economic impact of beach nourishment operations in Nice. Environmental rules of the French government require considering the impacts on the marine ecosystem. Therefore, practices need to evolve, but they also must be backed up by evidence from studies. In this scenario, the tracing experiment meets the expectations of the Municipality of Nice for both erosion control and in the environmental respect as the results provided promising insights on both these aspects, which are top priorities for the management of the Bay of Nice. This study is the first step towards a more efficient planning of beach nourishment and a better setup of the groin system on the west side of the bay. In addition, it contributes to better appreciate the short-term processes involved in the sediment loss offshore, which is the main cause driving periodic artificial nourishment on Nice beach.

Currently, the sediment used to refill the beach comes from a local quarry in south-eastern France. The pebbles are only selected according to their lithology and grain-size. However, this study shows that reducing the quantity of spherical pebbles in favor of disk-shaped ones can limit the offshore shift and ultimately beach erosion, as the results clearly documented that short-term processes may also lead to berm-rebuilding. With this in mind, defining the transport patterns of pebbles of this size is crucial because they are comparable in size to those generally used during beach nourishment operations. Local managers assess the conformity of a beach fill material according to specific grain-size thresholds:

- **< 0.1 mm**: A minimum of these materials is required; a quantity greater than 2% of this category will result in the rejection of the material proposed.
- **Between 0.1 mm and 2 mm**: A minimum of these materials is required; a quantity greater than 20% of this category will result in the rejection of the material proposed.
- **Between 2 mm and 20 mm**: A minimum of these materials is required; a quantity greater than 30% of this category will result in the rejection of the material proposed.
- **Between 20 mm and 80 mm**: A maximum of these materials is desired; a quantity of less than 50% of this category will result in the rejection of the material proposed.
- **80 mm**: A minimum of these materials is required; a quantity greater than 5% of this category will result in the rejection of the material proposed.

Since the results show that mass is not a factor that leads to particular transport trends, the reported size thresholds do not need adjustment or variation. Optimizing these interventions means understanding pebble behaviors, especially in early stages after introduction. Similarly, improved beach nourishment operations would also have environmental repercussions because the reduction of offshore sediment losses would also reduce the impact on seabed grass such as *Posidonia* and *Cymodocea*, whose development is adversely affected by the heavy presence of coarse sediment. Even if better-optimized pebbles cost more by weight, they will require less volume to compensate for offshore loss.

In addition, to improve the sediment management along the Bay of Nice, the Municipality aims at replicating this experiment on a larger scale to confirm the findings of our short-term observations. We envision carrying out an injection of tracers for a medium- (1 month) and long-term (3 months) experiment to gather more data about extended fair-weather periods, but also including high-energy events. In this way the offshore sediment loss processes would be unveiled too. The by-product of the longer-term experiment would be ensuring that these transport patterns could also be observed outside of the groin system. Ultimately, we could provide the necessary information to adapt beach nourishment operations in terms of sediment quality and quantity, target more specific areas and harmonize the western groin system with the new sediment management. In addition, the recommendations here suggested for beach management in Nice may also be valid for many other sites on the French Mediterranean coast, considering the high percentage of natural and artificial coarse-clastic beaches along the French Riviera, most of which are subject to erosion processes similar to those found in Nice (Anthony, 1994).

6. Conclusions

The results of the short-term tracing experiment carried out in a beach compartment along the Bay of Nice confirm some of the findings previous investigations pointed out about coarse-clastic beach transport processes: i) the swash zone is where tagged pebbles are often lost, which means that coarse sediments move throughout it both in the longshore and cross-shore directions; ii) the step crest is where most of the tagged pebbles are detected as many marked pebbles roll down the beachface until they stop there; iii) disk-shaped pebbles respond less promptly to downslope movement than spheres, but experience far longshore displacements. However, this research also shows an uncharacteristic trend compared to other coarse sediment tracing experiments: the tracer recovery rate was poor after the first survey but spiked after 24 h. This development is explained by early destruction of the fair-weather berm while the water level still reached the upper part of the swash zone and the base of the berm, and the ensuing rebuilding under the combination of rising tide and increasing wave motion. The presence of such a process is crucial for Fabron beach, and all the compartments along the Bay of Nice, because it proves that coarse sediments do not just move downslope under whichever wave state; when the wave motion is mild, they can be pushed back up to rebuild the fair-weather berm without evidence of volume loss. Loss begins when the water level reaches the higher part of the backshore, even though some of the volumes are just transferred longshore throughout the beach as rotation processes unfold.

These detailed insights about the short-term behavior of the Fabron beach might serve as an indication of the processes acting in the long-term at least during fair-weather periods. While size does not affect transport patterns, shape surely does. Clearly, high-energy events still dictate the fate of the beach along the Bay of Nice. However, this study under mild wave conditions and different transport pathways between shapes in the short-term can lead to long-term benefits in the way the beach compartments are managed. Based on this study's results, using disk-shaped pebbles as beach fill material during replenishment would likely result in longer-lived nourishments for the targeted compartment, providing benefits to stakeholders in both economic and environmental terms.

CRediT authorship contribution statement

Duccio Bertoni: Writing – original draft, Validation, Investigation, Funding acquisition, Data curation, Conceptualization. **Silas Dean:** Writing – review & editing, Visualization, Software, Methodology. **Alessandro Pozzebon:** Validation, Methodology, Investigation, Conceptualization. **Rémi Dumasdelage:** Writing – review & editing, Software, Methodology, Investigation, Data curation. **Julien Larraun:** Writing – review & editing, Software, Methodology, Investigation, Data curation. **Giovanni Sarti:** Writing – review & editing, Methodology, Conceptualization.

Declaration of competing interest

The authors declare that they have no known competing financial interests or personal relationships that could have appeared to influence the work reported in this paper.

Data availability

Data will be made available on request.

Acknowledgements

Special thanks go to Giacomo Bruno, Marcello Giannuoli, and Leonardo Salvadori for their support during the recovery campaigns at Nice. We also appreciated Pietro Giacomini's contribution while sorting out the huge amount of data that have been acquired throughout the experiment. The observations made by two anonymous reviewers significantly improved the manuscript: we sincerely thank them for their time and effort. The research was financed by personal funds granted to Duccio Bertoni by UniPI (Fondi Ateneo 2019).

Appendix A. Supplementary data

Supplementary data to this article can be found online at https://doi.org/10.1016/j.ocecoaman.2024.107157.

References

Allan, J.C., Hart, R., Tranquilli, J.V., 2006. The use of Passive Integrated Transponder (PIT) tags to trace cobble transport in a mixed sand-and-gravel beach on the high-energy Oregon coast, USA. Mar. Geol. 232, 63–86. https://doi.org/10.1016/j.margeo.2006.07.005.

Almeida, L.P., Masselink, G., Russell, P.E., Davidson, M.A., 2015. Observations of gravel beach dynamics during high energy wave conditions using a laser scanner. Geomorphology 228, 15–27. https://doi.org/10.1016/j.geomorph.2014.08.019.

Anthony, E.J., 1994. Natural and artificial shores of the French Riviera: an analysis of their Interrelationship. J. Coast Res. 10, 48–58.

Anthony, E.J., 1997. The status of beaches and shoreline development options on the French Riviera: a perspective and a prognosis. J. Coast Conserv. 3, 169–178. https://doi.org/10.1007/BF02908192.

Anthony, E.J., Cohen, O., Sabatier, F., 2011. Chronic offshore loss of nourishment on Nice beach, French Riviera: a case of over-nourishment of a steep beach? Coast. Eng. 58, 374–383 j.coastaleng.2010.11.001.

Anthony, E.J., Julian, M., 1999. Source-to-sink sediment transfers, environmental engineering and hazard mitigation in the steep Var River catchment, French Riviera, southeastern France. Geomorphology 31, 337–354. https://doi.org/10.1016/S0169-555X(99)00088-4.

Barale, L., 2016. The early geological exploration of the Nice region (French Maritime Alps) in the late 18th–19th centuries. Proc. Geologists' Assoc. 127, 747–760. https://doi.org/10.1016/j.pgeola.2016.11.010.

Benelli, G., Pozzebon, A., Bertoni, D., Sarti, G., Ciavola, P., Grottoli, E., 2012. An Analysis of the Performances of Low Frequency Cylinder Glass Tags for the Underwater Tracking of Pebbles on a Natural Beach. Fourth International EURASIP Workshop on RFID Technology, RFID, pp. 72–77. https://doi.org/10.1109/RFID.2012.30, 2012.

Benelli, G., Pozzebon, A., Raguseo, G., Bertoni, D., Sarti, G., 2009. An RFID based system for the underwater tracking of pebbles on artificial coarse beaches. In: Proceedings of the Third International Conference on Sensor Technologies and Applications, SENSORCOMM 2009, pp. 294–299. https://doi.org/10.1109/SENSORCOMM.2009.52.

Bertoni, D., Dean, S., Trembanis, A.C., Sarti, G., 2020. Multi-month sedimentological characterization of the backshore of an artificial coarse-clastic beach in Italy. Rendiconti Lincei 31, 65–77. https://doi.org/10.1007/s12210-019-00852-2.

Bertoni, D., Grottoli, E., Ciavola, P., Sarti, G., Benelli, G., Pozzebon, A., 2013. On the displacement of marked pebbles on two coarse-clastic beaches during short fair-weather periods (Marina di Pisa and Portonovo, Italy). Geo Mar. Lett. 33, 463–476. https://doi.org/10.1007/s00367-013-0341-3.

Bertoni, D., Sarti, G., 2011. On the profile evolution of three artificial pebble beaches at Marina di Pisa, Italy. Geomorphology 130, 244–254. https://doi.org/10.1016/j.geomorph.2011.04.002.

Bertoni, D., Sarti, G., Benelli, G., Pozzebon, A., Raguseo, G., 2012. Transport trajectories of "smart" pebbles on an artificial coarse-grained beach at Marina di Pisa (Italy): Implications for beach morphodynamics. Mar. Geol. 291–294, 227–235. https://doi.org/10.1016/j.margeo.2011.08.004.

Buscombe, D., 2013. Transferable wavelet method for grain-size distribution from images of sediment surfaces and Thin sections, and other natural Granular patterns. Sedimentology 60, 1709–1732. https://doi.org/10.1111/sed.12049.

Buscombe, D., Masselink, G., 2006. Concepts in gravel beach dynamics. Earth Sci. Rev. 79, 33–52. https://doi.org/10.1016/j.earscirev.2006.06.003.

Cappucci, S., Bertoni, D., Cipriani, L.E., Boninsegni, G., Sarti, G., 2020. Assessment of the anthropogenic sediment budget of a littoral cell system (Northern Tuscany, Italy). Water 12, 3240. https://doi.org/10.3390/w12113240.

Casamayor, M., Alonso, I., Valiente, N.G., Sanchez-Garcia, M.J., 2022. Seasonal response of a composite beach in relation to wave climate. Geomorphology 408, 108245. https://doi.org/10.1016/j.geomorph.2022.108245.

Cervantes, O., Espejel, I., Arellano, E., Delhumeau, S., 2008. Users' perception as a tool to improve urban beach planning and management. Environ. Manag. 42, 249–264. https://doi.org/10.1007/s00267-008-9104-8.

Cooke, B., Jones, A.R., Goodwin, I.D., Bishop, M.J., 2012. Nourishment practices on Australian sandy beaches: a review. J. Environ. Manag. 113, 319–327. https://doi.org/10.1016/j.jenvman.2012.09.025.

Curtiss, G.M., Osborne, P.D., Horner-Devine, A.R., 2009. Seasonal patterns of coarse sediment transport on a mixed sand and gravel beach due to vessel wakes, wind waves, and tidal currents. Mar. Geol. 259, 73–85. https://doi.org/10.1016/j.margeo.2008.12.009.

Cuttler, M.V.W., Lowe, R.J., Falter, J.L., Buscombe, D., 2017. Estimating the settling velocity of bioclastic sediment using common grain-size analysis techniques. Sedimentology 64, 987–1004. https://doi.org/10.1111/sed.12338.

de Schipper, M.A., Ludka, B.C., Raubenheimer, B., Luijendijk, A.P., Schlacher, T.A., 2021. Beach nourishment has complex implications for the future of sandy shores. Nat. Rev. Earth Environ. 2, 70–84. https://doi.org/10.1038/s43017-020-00109-9.

Dickson, M.E., Kench, P.S., Kantor, M.S., 2011. Longshore transport of cobbles on a mixed sand and gravel beach, southern Hawke Bay, New Zealand. Mar. Geol. 287, 31–42. https://doi.org/10.1016/j.margeo.2011.06.009.

Dubar, M., Anthony, E.J., 1995. Holocene environmental change and river-mouth sedimentation in the Baie des Anges, French Riviera. Quat. Res. 43, 329–343. https://doi.org/10.1006/qres.1995.1039.

Dumasdelage, R., Delestre, O., Clamond, D., Bonnin, A., Moretti, M., Ceruti, P., Gourbesville, P., 2014. Numerical Modeling of the erosion phenomena on Nice shoreface using TELEMAC system. Book of Proceedings of the Third IAHR Europe Congress, Porto (Portugal), 10650.

Dumasdelage, R., Delestre, O., Clamond, D., Gourbesville, P., 2016. Storm events of Nice bay: a numerical modeling of the interactions between wave, current, and solid transport. In: Gourbesville, P., Cunge, J., Caignaert, G. (Eds.), Advances in Hydroinformatics. Springer Water. Springer, Singapore, pp. 17–27. https://doi.org/10.1007/978-981-287-615-7_2.

EDF R&D, 2011. TOMAWAC – Software for Sea State Modelling on Unstructured Grids over Oceans and Coastal Seas. In: Release, 6.1. EDF, Paris.

Elko, N., Roberts Briggs, T., Benedet, L., Robertson, Q., Thomson, G., Webb, B.M., Garvey, K., 2021. A century of U.S. beach nourishment. Ocean Coast Manag. 199, 105406 https://doi.org/10.1016/j.ocecoaman.2020.105406.

Eyal, H., Enzel, Y., Meiburg, E., Vowinckel, B., Lensky, N.G., 2021. How does coastal gravel get sorted under stormy longshore transport? Geophys. Res. Lett. 48, e2021GL095082 https://doi.org/10.1029/2021GL095082.

French, P.W., 2001. Coastal Defences: Processes, Problems and Solutions. Routledge, London.

García-Morales, G., Arreola-Lizárraga, J.A., Rosales Grano, P., 2018. Integrated assessment of recreational quality and carrying capacity of an urban beach. Coast. Manag. 46, 316–333. https://doi.org/10.1080/08920753.2018.1474070.

Goda, Y., 2000. Random Seas and Design of Maritime Structures In: Advanced Series on Ocean Engineering, second ed., vol. 15. World Scientific, Singapore. https://doi.org/10.1142/3587.

Grottoli, E., Bertoni, D., Ciavola, P., Pozzebon, A., 2015. Short term displacements of marked pebbles in the swash zone: focus on particle shape and size. Mar. Geol. 367, 143–158. https://doi.org/10.1016/j.margeo.2015.06.006.

Grottoli, E., Bertoni, D., Ciavola, P., 2017. Short- and medium-term response to storms on three Mediterranean coarse-grained beaches. Geomorphology 295, 738–748. https://doi.org/10.1016/j.geomorph.2017.08.007.

Grottoli, E., Bertoni, D., Pozzebon, A., Ciavola, P., 2019. Influence of particle shape on pebble transport in a mixed sand and gravel beach during low energy conditions: implications for nourishment projects. Ocean Coast Manag. 169, 171–181. https://doi.org/10.1016/j.ocecoaman.2018.12.014.

Han, M., Yang, D.Y., Yu, J., Kim, J.W., 2017. Typhoon impact on a pure gravel beach as assessed through gravel movement and topographic change at yeocha beach, south coast of korea. J. Coast Res. 33, 889–906. https://doi.org/10.2112/JCOASTRES-D-16-00104.1.

Hanson, H., Brampton, A., Capobianco, M., Dette, H.H., Hamm, L., Laustrup, C., Lechuga, A., Spanhoff, R., 2002. Beach nourishment projects, practices, and objectives—a European overview. Coast. Eng. 47, 81–111. https://doi.org/10.1016/S0378-3839(02)00122-9.

Hayes, M.O., Michel, J., Betenbaugh, D.V., 2010. The intermittently exposed, coarse grained gravel beaches of Prince William Sound, Alaska: comparison with open-ocean gravel beaches. J. Coast Res. 26 (1), 4–30. https://doi.org/10.2112/08-1071.

Ions, K., Karunarathna, H., Reeve, D.E., Pender, D., 2021. Gravel barrier beach morphodynamic response to extreme conditions. J. Mar. Sci. Eng. 9, 135. https://doi.org/10.3390/jmse9020135.

Jolivet, M., Anthony, E.J., Gardel, A., Maury, T., Morvan, S., 2022. Dynamics of mud banks and sandy urban beaches in French Guiana, South America. Reg. Environ. Change 22, 101. https://doi.org/10.1007/s10113-022-01944-w.

Karunarathna, H., Horrillo-Caraballo, J.M., Ranasinghe, R., Short, A.D., Reeve, D.E., 2012. An analysis of the cross-shore beach morphodynamics of a sandy and a composite gravel beach. Mar. Geol. 299–302, 33–42. https://doi.org/10.1016/j.margeo.2011.12.011.

Kemp, L., Xu, C., Depledge, J., Ebi, K.L., Gibbins, G., Kohler, T.A., Rockström, J., Scheffer, M., Schellnhuber, H.J., Steffen, W., Lenton, T.M., 2022. In: Proceedings of the National Academy of Sciences, vol. 119, e2108146119. https://doi.org/10.1073/pnas.2108146119.

Komen, G.J., Cavaleri, L., Donelan, M., Hasselmann, K., Hasselmann, S., Janssen, P.A.E. M., 1994. Dynamics and Modelling of Ocean Waves. Cambridge University Press, Cambridge. https://doi.org/10.1017/CBO9780511628955.

Kumada, T., Uda, T., Matsu-ura, T., Sumiya, M., 2010. Field experiment on beach nourishment using gravel at Jinkoji Coast. In: Proceedings of the 32nd International Conference on Coastal Engineering, vol. 2010. ICCE, 91524.

López, I., Aragonés, L., Villacampa, Y., Navarro-González, F.J., 2018. Gravel beaches nourishment: modelling the equilibrium beach profile. Sci. Total Environ. 619–620, 772–783. https://doi.org/10.1016/j.scitotenv.2017.11.156.

Luo, S., Liu, Y., Jin, R., Zhang, J., Wei, W., 2016. A guide to coastal management: benefits and lessons learned of beach nourishment practices in China over the past two decades. Ocean Coast Manag. 134, 207–215. https://doi.org/10.1016/j.ocecoaman.2016.10.011.

McCall, R.T., Masselink, G., Poate, T.G., Roelvink, J.A., Almeida, L.P., 2015. Modelling the morphodynamics of gravel beaches during storms with XBeach-G. Coast. Eng. 103, 52–66. https://doi.org/10.1016/j.coastaleng.2015.06.002.

Miller, I.M., Warrick, J.A., Morgan, C., 2011. Observations of coarse sediment movements on the mixed beach of the Elwha Delta, Washington. Mar. Geol. 282, 201–214. https://doi.org/10.1016/j.margeo.2011.02.012.

Morris, R.L., Konlechner, T.M., Ghisalberti, M., Swearer, S.E., 2018. From grey to green: efficacy of eco-engineering solutions for nature-based coastal defence. Global Change Biol. 24, 1827–1842. https://doi.org/10.1111/gcb.14063.

Moss, A.J., 1962. The physical nature of common sandy and pebbly deposits: Part I. Am. J. Sci. 260, 337–373. https://doi.org/10.2475/ajs.260.5.337.

Moss, A.J., 1963. The physical nature of common sandy and pebbly deposits: Part II. Am. J. Sci. 261, 197–243. https://doi.org/10.2475/ajs.261.4.297.

Muhajjir, M., Suga, H., Aoki, S., 2019. An experimental study on cross-shore morphodynamics of a composite sand-gravel beach. In: Proceedings of the 29th International Ocean and Polar Engineering Conference. Honolulu (USA), June 16-19, 2019.

Orford, J.D., Forbes, D.L., Jennings, S.C., 2002. Organisational controls, typologies and time scales of paraglacial gravel-dominated coastal systems. Geomorphology 48, 51–85. https://doi.org/10.1016/S0169-555X(02)00175-7.

Parkinson, R.W., Ogurcak, D.E., 2018. Beach nourishment is not a sustainable strategy to mitigate climate change. Estuar. Coast Shelf Sci. 212, 203–209. https://doi.org/10.1016/j.ecss.2018.07.011.

Pikelj, K., Ružić, I., Ilić, S., James, M.R., Kordić, B., 2018. Implementing an efficient beach erosion monitoring system for coastal management in Croatia. Ocean Coast Manag. 156, 223–238. https://doi.org/10.1016/j.ocecoaman.2017.11.019.

Pinto, C.A., Silveira, T.M., Teixeira, S.B., 2020. Beach nourishment practice in mainland Portugal (1950–2017): overview and retrospective. Ocean Coast Manag. 192, 105211 https://doi.org/10.1016/j.ocecoaman.2020.105211.

Pranzini, E., Anfuso, G., Cinelli, I., Piccardi, M., Vitale, G., 2018. Shore protection structures increase and evolution on the northern tuscany coast (Italy): influence of tourism industry. Water 10, 1647. https://doi.org/10.3390/w10111647.

Pupin, J.P., Fernex, F., Chassefiere, B., Bernat, M., Di Lauro, A., Ferrand, J.L., 2001. Impact des politiques de planification et d'aménagement sur les côtes urbanisées à vocation touristiques, p. 308. Unpublished report, Programme Nicomède, Projet "Ligurimpact", INTERREG II, Tome II.

Rodella, I., Madau, F., Mazzanti, M., Corbau, C., Carboni, D., Utizi, K., Simeoni, U., 2019. Willingness to pay for management and preservation of natural, semi-urban and urban beaches in Italy. Ocean Coast Manag. 172, 93–104. https://doi.org/10.1016/j.ocecoaman.2019.01.022.

Ruiz de Alegria-Arzaburu, A., Masselink, G., 2010. Storm response and beach rotation on a gravel beach, Slapton Sands, U.K. Mar. Geol. 278, 77–99. https://doi.org/10.1016/j.margeo.2010.09.004.

Russell, P.E., Masselink, G., Blenkinsopp, C., Turner, I.L., 2009. A comparison of berm accretion in the swash zone on sand and gravel beaches at the timescale of individual waves. J. Coast Res. SI56, 1791–1795.

Schoonees, T., Gijón Mancheño, A., Scheres, B., Bouma, T.J., Silva, R., Schlurmann, T., Schüttrumpf, H., 2019. Hard structures for coastal protection, towards greener designs. Estuar. Coast 42, 1709–1729. https://doi.org/10.1007/s12237-019-00551-z.

Scott, T., Masselink, G., O'Hare, T., Saulter, A., Poate, T., Russell, P., Davidson, M., Conley, D., 2016. The extreme 2013/2014 winter storms: beach recovery along the southwest coast of England. Mar. Geol. 382, 224–241. https://doi.org/10.1016/j.margeo.2016.10.011.

SOGREAH, 2009. Littoral entre Antibes et Cap d'Ail, bilan, analyse et préconisation sur le phénomène érosif. Contrat de Baie d'Antibes à Cap d'Ail. Fascicule n°6 Nice, p. 102. Ref. 1711764.

Soloy, A., Turki, I., Lecoq, N., Lopez Solano, C., Laignel, B., 2022. Spatio-temporal variability of the morpho-sedimentary dynamics observed on two gravel beaches in response to hydrodynamic forcing. Mar. Geol. 447, 106796 https://doi.org/10.1016/j.margeo.2022.106796.

Stark, N., Hay, A.E., 2016. Pebble and cobble transport on a steep, mega-tidal, mixed sand and gravel beach. Mar. Geol. 382, 210–223. https://doi.org/10.1016/j.margeo.2016.10.012.

Tadić, A., Ružić, I., Krvavica, N., Ilić, S., 2022. Post-nourishment changes of an artificial gravel pocket beach using UAV imagery. J. Mar. Sci. Eng. 10, 358. https://doi.org/10.3390/jmse10030358.

Wiggins, M., Scott, T., Masselink, G., McCarroll, R.J., Russell, P., 2020. Predicting beach rotation using multiple atmospheric indices. Mar. Geol. 426, 106207 https://doi.org/10.1016/j.margeo.2020.106207.

Zingg, T., 1935. Beitrag zur Schotteranalyse. ETH, Zürich (Switzerland), p. 141. https://doi.org/10.3929/ethz-a-000103455. PhD thesis.